Quenched SU(2) adjoint scalar propagator in minimal Landau gauge

Axel Maas

Institute of Physics, NAWI Graz, University of Graz, Universitätsplatz 5, A-8010 Graz, Austria

(Received 9 January 2019; published 20 March 2019)

It is a longstanding question whether the confinement of matter fields in QCD has an imprint in the (gauge-dependent) correlation functions, especially the propagators. In particular, in the quenched case, a fundamental difference could be expected between adjoint and fundamental matter. In a preceding investigation, the propagator of a fundamental scalar was studied, showing no obvious sign of confinement. Here, as a complement, the adjoint scalar propagator is investigated over a wide range of parameters in the minimal Landau gauge using lattice gauge theory. This study is performed in two, three, and four dimensions in quenched SU(2) Yang-Mills theory, both in momentum space and position space. No conclusive difference between the two cases is found.

DOI: 10.1103/PhysRevD.99.054504

I. INTRODUCTION

The confinement[1] of matter in QCD is a very long-standing problem [1]. In particular, it is especially unclear how to read off the confinement of a particle from its elementary correlation functions. This could be both the propagator as well as the vertices [2–8]. Of course, the correlation functions describing the elementary particles, matter and gluon alike, are gauge dependent. Thus, this question requires fixing a gauge, and thus the answer is potentially gauge dependent. Here, this question will be posed in a particular case, the best-studied one so far, the Landau gauge, in particular the so-called minimal Landau gauge [3].

A natural quantity to investigate these questions is the spectral density. This spectral density is found to be positivity violating for gluons [2–10]. However, the precise form this violation takes, e.g., by a nontrivial cut structure, complex poles, or otherwise, is not entirely settled. At any rate, any such violation of positivity immediately implies that the particle cannot be part of the physical state space, and thus not observable. Sufficient, but not necessary, conditions for violation of positivity can be either a nonpositive definite position-space correlation function or a nonmonotonous behavior of the derivatives of the momentum-space correlation functions [3]. If the correlation function is known both in momentum space and position space sufficiently well, these results can be used to constrain the type of analytic structure. For example, an oscillatory behavior in position space and screened behavior in momentum space points to a complex pole structure [3].

Results for fermionic matter, especially quarks, are intricate, see [2,8,11–13]. However, the results are compatible with a violation of positivity also in fermion propagators. This is true for quarks both in the adjoint and the fundamental representation.

Scalar matter suggests itself as a testbed of this question,[2] due to the simpler Lorentz structure. For scalar matter in the fundamental representation there have been various suggestions for its behavior, which have been obtained using continuum methods [15–22]. On the lattice a violation of positivity has been found, though it is not entirely clear whether its remains in the continuum and infinite-volume limit [23]. Still, the propagator showed the presence of an intrinsic, nonzero mass scale even if massless at tree-level, and consequently exhibits a momentum-space propagator similar to that of a massive particle. Thus, there is no clear indication for confinement in the fundamental scalar sector.

On the other hand, it is naively expected that adjoint scalar matter could show a different behavior in the quenched case [16,22]. After all, the Wilson string tension of the adjoint string still vanishes, due to string-breaking by

[1]Confinement is here understood, if not noted otherwise, in the sense that a particle cannot be observed as an asymptotic, physical state. In this sense, also, QCD is confining. A definition of confinement based on the Wilson string tension is in no obvious way related to this. In fact, according to the Wilson string tension, QCD is not a confining theory. See [1] for a more detailed discussion of this difference.

[2]There are multiple subtleties with respect to this question in the dynamical theory due to the possibility of a Brout-Englert-Higgs effect, see [14]. In the present quenched case, this is not relevant.

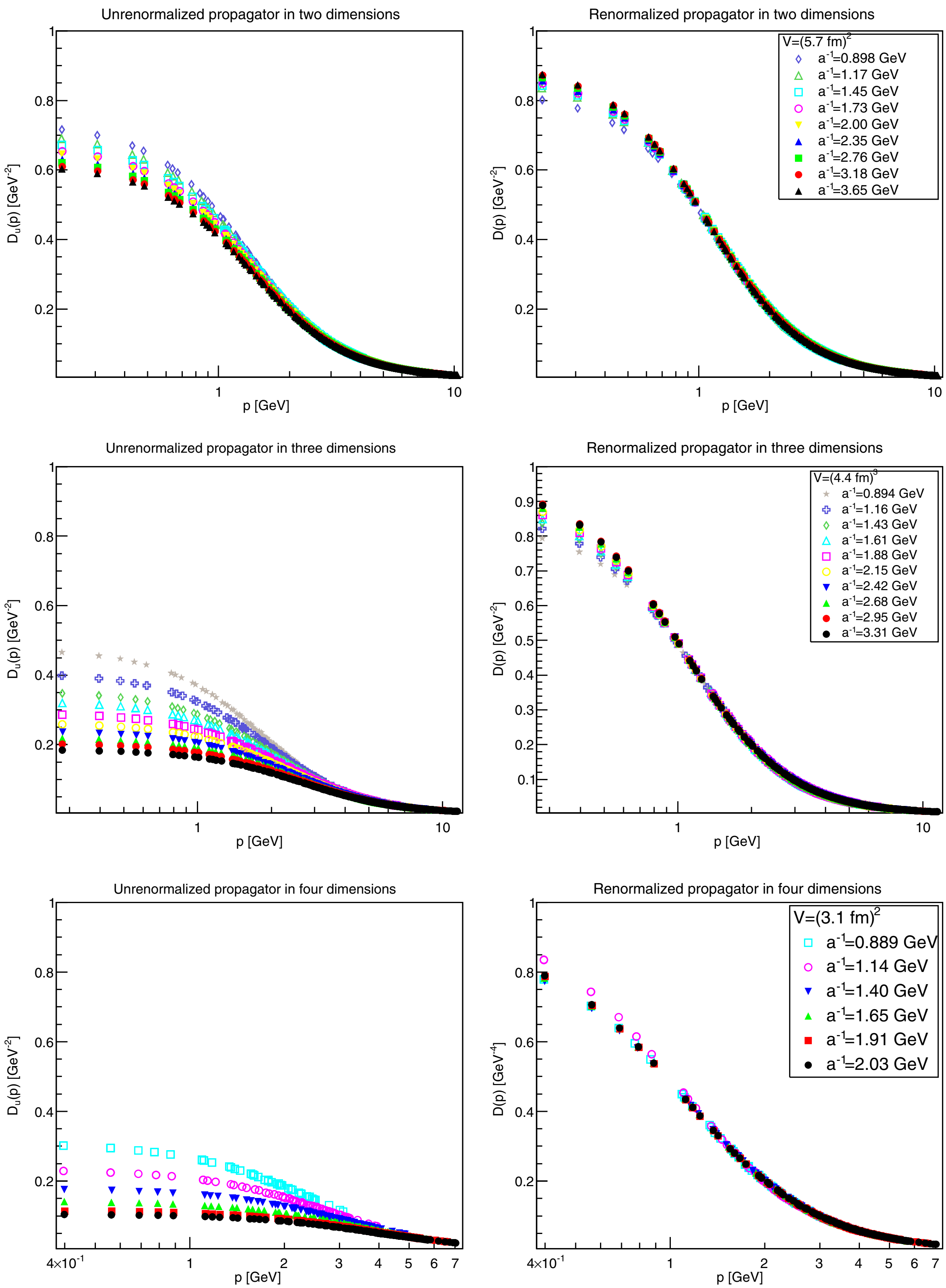

FIG. 1. Unrenormalized propagator (left panels) and renormalized propagator (right panels). The top panels are for two dimensions, the middle panels for three dimensions, and the bottom panels for four dimensions. The values are $m_r = m = 1$ GeV and $\mu = 1.5$ GeV. If the (statistical 1σ) error bars here and hereafter are not visible then they are smaller than the symbol size.

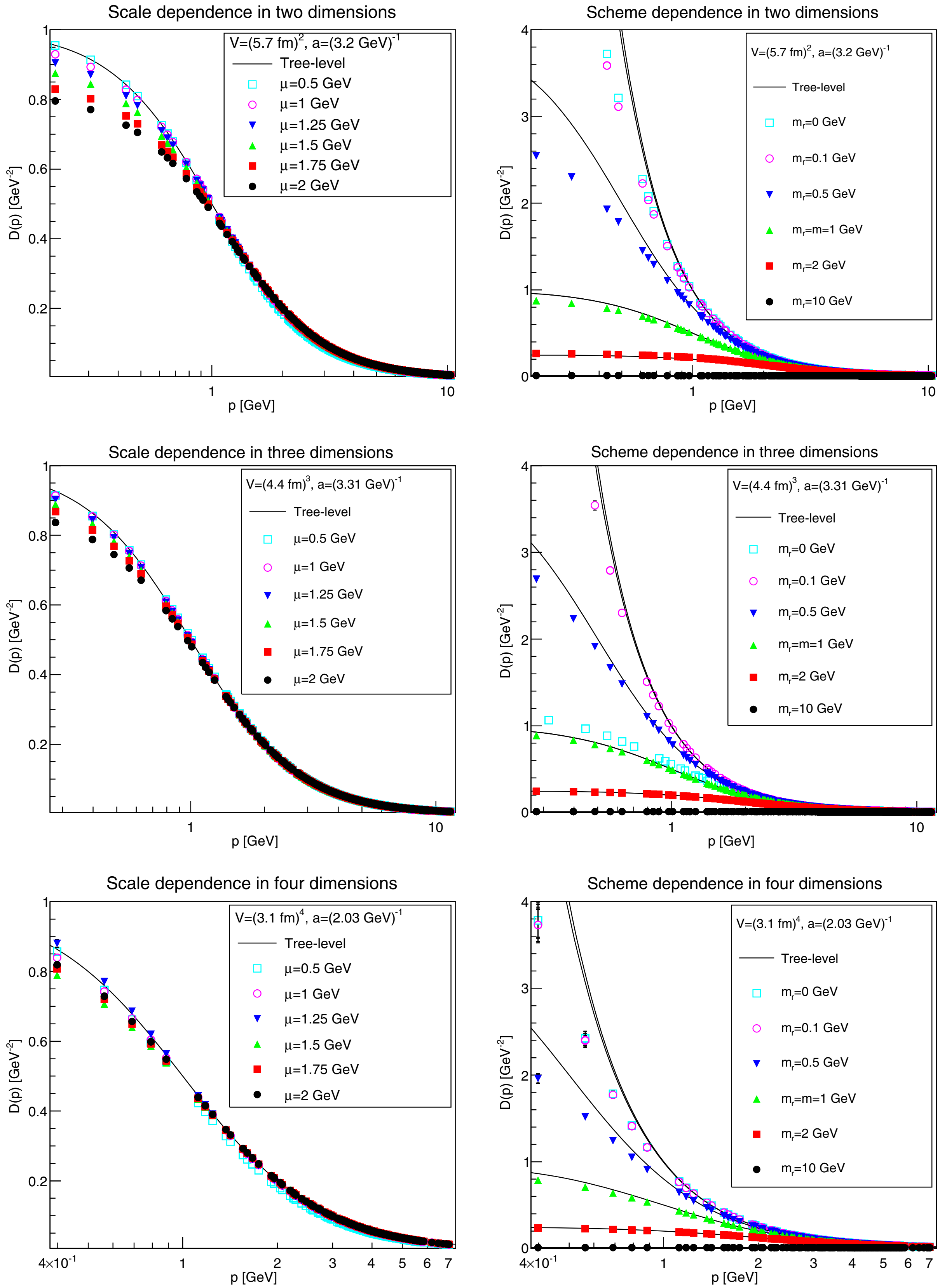

FIG. 2. Scale dependence at $m_r = m = 1$ GeV (left panels) and scheme dependence at $\mu = 1.5$ GeV (right panels) of the renormalized propagator. The top panels are two dimensions, the middle panels three dimensions, and the bottom panels four dimensions. The tree-level propagator is shown for comparison as a full line.

matter-gluon hybrids. In case of the quarks, this does not seem to lead to a differing behavior for the propagator at a qualitative level [13,24–26]. However, adjoint quarks have also a very different behavior when it comes to chiral symmetry breaking, as their differing finite-temperature behavior shows [27–29]. This may interfere with a clear picture. Therefore, once more, it becomes interesting to study adjoint scalar matter in the quenched case.

This will be done here. Following [23], this will be done for a wide range of lattice parameters, and for two, three, and four dimensions. Considering two dimensions may seem odd at first. However, in this case the violation of positivity for gluons appears similarly as in more dimensions [10,30–32]. But gluons are not dynamical but only pure gauge in two dimensions. At the same time, a confinement according to the Wilson potential occurs already for purely geometrical reasons [33]. Scalar particles are, however, also dynamical in two dimensions. In the fundamental case, this did not lead to any qualitative impact [23], and scalar matter behaved in the same way in all dimensions. It is, therefore, interesting to have a look at two dimensions.

Three dimensions take an intermediate position. While it is a dynamical theory in the quenched case, it has different

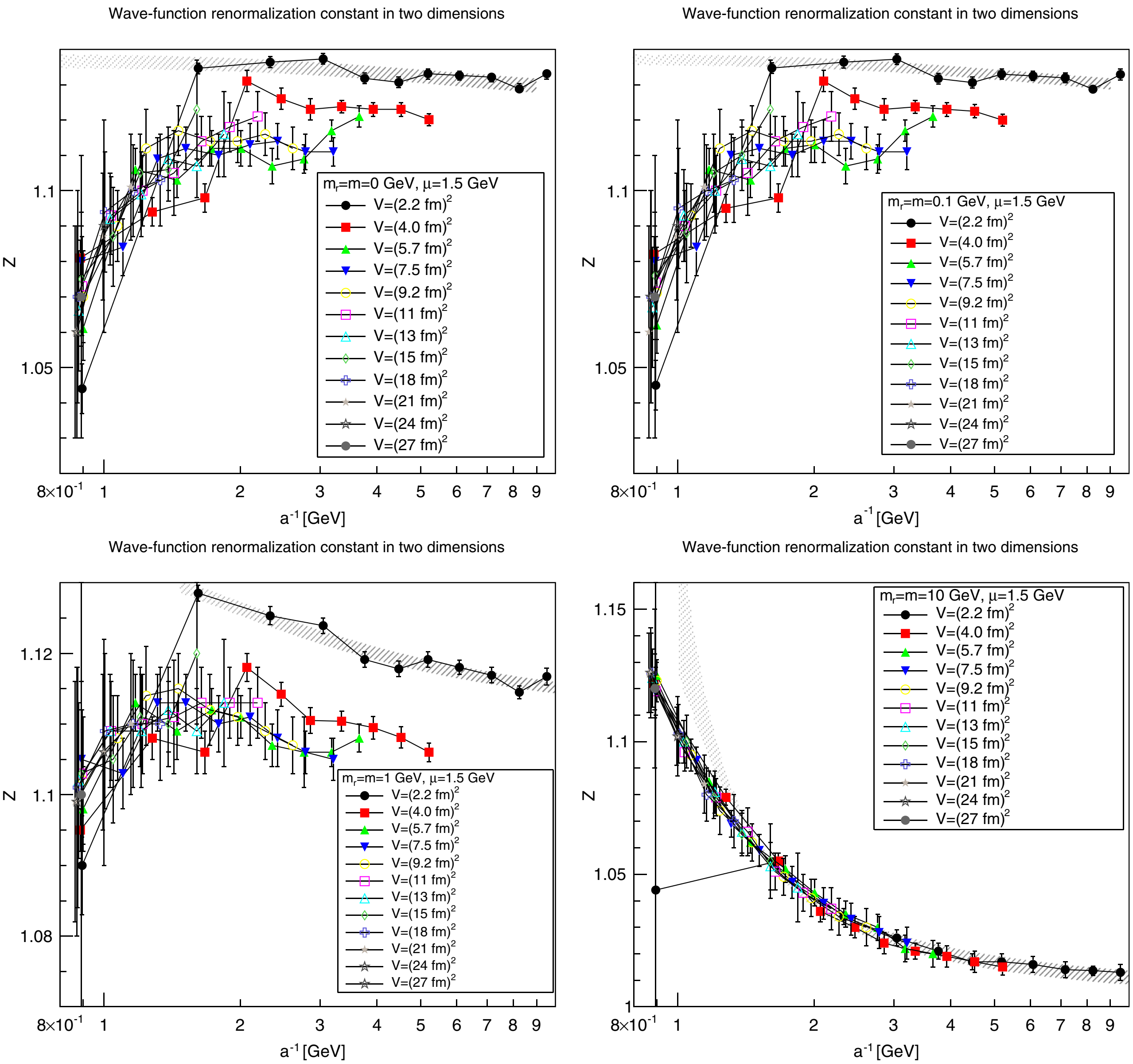

FIG. 3. The wave-function renormalization constant as a function of the lattice cutoff and the lattice volume in two dimensions for $\mu = 1.5$ GeV. The top-left panel shows the case of $m = m_r = 0$ GeV, the top-right panel of $m = m_r = 0.1$ GeV, the bottom-left panel of $m = m_r = 1$ GeV, and the bottom-right panel of $m = m_r = 10$ GeV. The hatched band is the fit (5) with the parameters given in Table I.

renormalization properties than in four dimensions. Moreover, while the four-dimensional unquenched case is potentially trivial, this is not true in three dimensions [34]. This could have potentially impact as well.

Again, as in [23], the quenched calculation will also help to understand lattice artifacts and renormalization properties of the scalar propagator beyond perturbation theory. This is helpful in studies of the dynamical case, which will, e.g., be relevant for studies of many kinds of grand-unified theories on the lattice [14], for which a host of predictions await nonperturbative precision tests [35] after exploratory investigations in the past [36,37].

As technically the study of the adjoint propagator is quite similar to the study of the fundamental propagator, this paper follows closely [23]. The technical setup is given in Sec. II. Renormalization is studied in detail in Sec. III. The results in momentum and position space are presented in Sec. IV. These are the main results of this work. A short summary follows in Sec. V. Some preliminary results have been presented in [20].

II. TECHNICAL SETUP

In the following, the propagator of a scalar particle in the adjoint representation of SU(2) in the quenched theory will

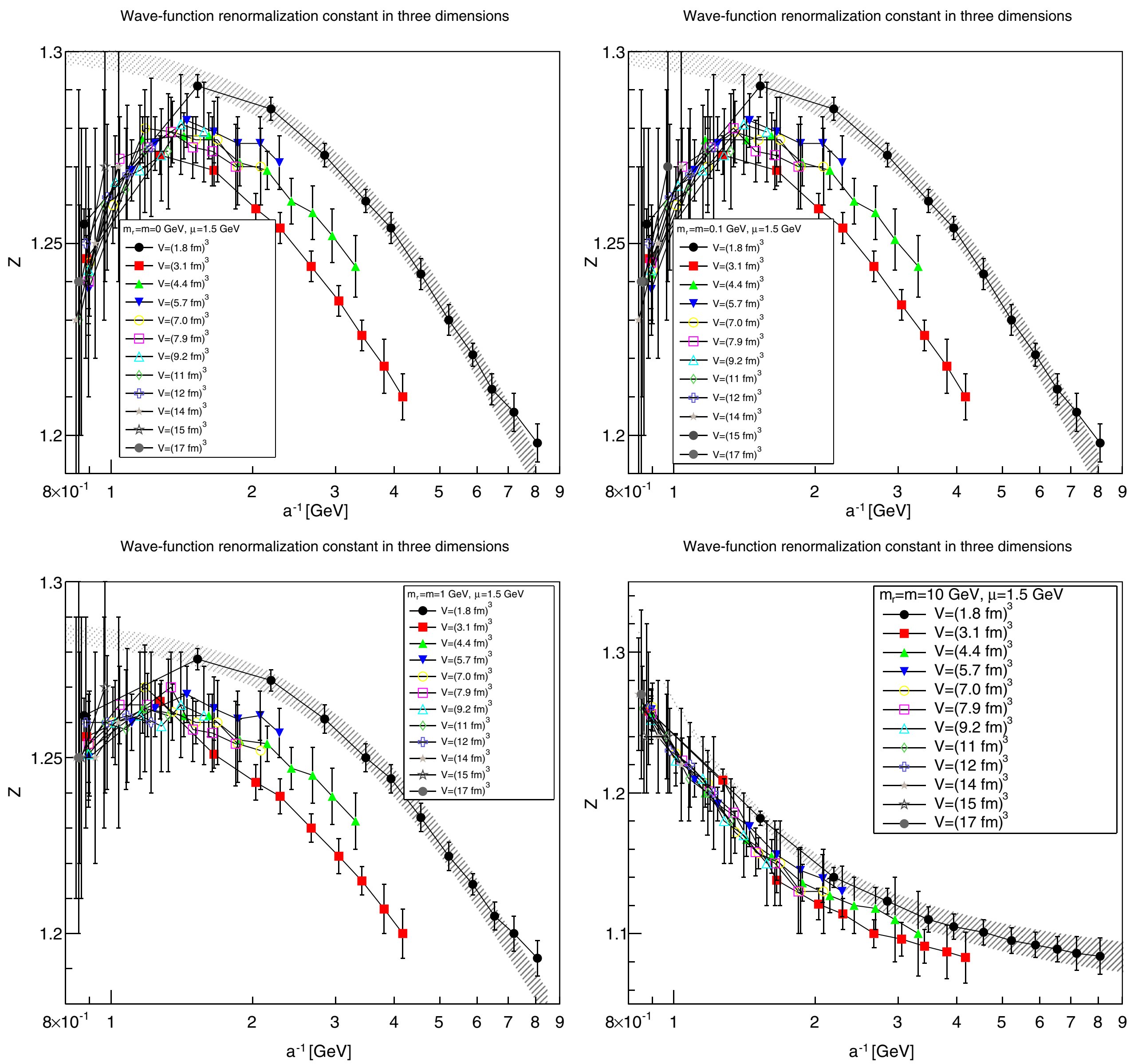

FIG. 4. The wave-function renormalization constant as a function of the lattice cutoff and the lattice volume in three dimensions for $\mu = 1.5$ GeV. The top-left panel shows the case of $m = m_r = 0$ GeV, the top-right panel of $m = m_r = 0.1$ GeV, the bottom-left panel of $m = m_r = 1$ GeV, and the bottom-right panel of $m = m_r = 10$ GeV. The hatched band is the fit (5) with the parameters given in Table I.

be determined in two, three, and four dimensions. The technical setup is based on [23,30,38,39]. Thus, the gauge action is the Wilson action for SU(2) Yang-Mills theory. The gauge field configurations are obtained using a cycle of heatbath and overrelaxation updates. The lattice setups are listed in Table III in Appendix. The determination of the lattice spacing has been performed as in [32].

Note that the limiting factor in terms of lattice volumes has been the required amount of statistics, especially for the position-space investigation. Though the Schwinger function is found to be positivity-violating in Sec. III C, it still shows (additional) exponential suppression at large times. Since smearing alters the momentum-space properties drastically [40], this can only be beaten by an exponential increase in statistics. Hence, the present investigation is primarily statistics limited. In the same vein, physically small volumes were thus the only possibility to reach the large momenta necessary to investigate the logarithmic behavior of the renormalization constants in Sec. III.

Each decorrelated configuration is fixed to minimal Landau gauge [3] using adaptive stochastic overrelaxation [38]. The quenched adjoint propagator has been obtained in a similar fashion as the quenched fundamental one

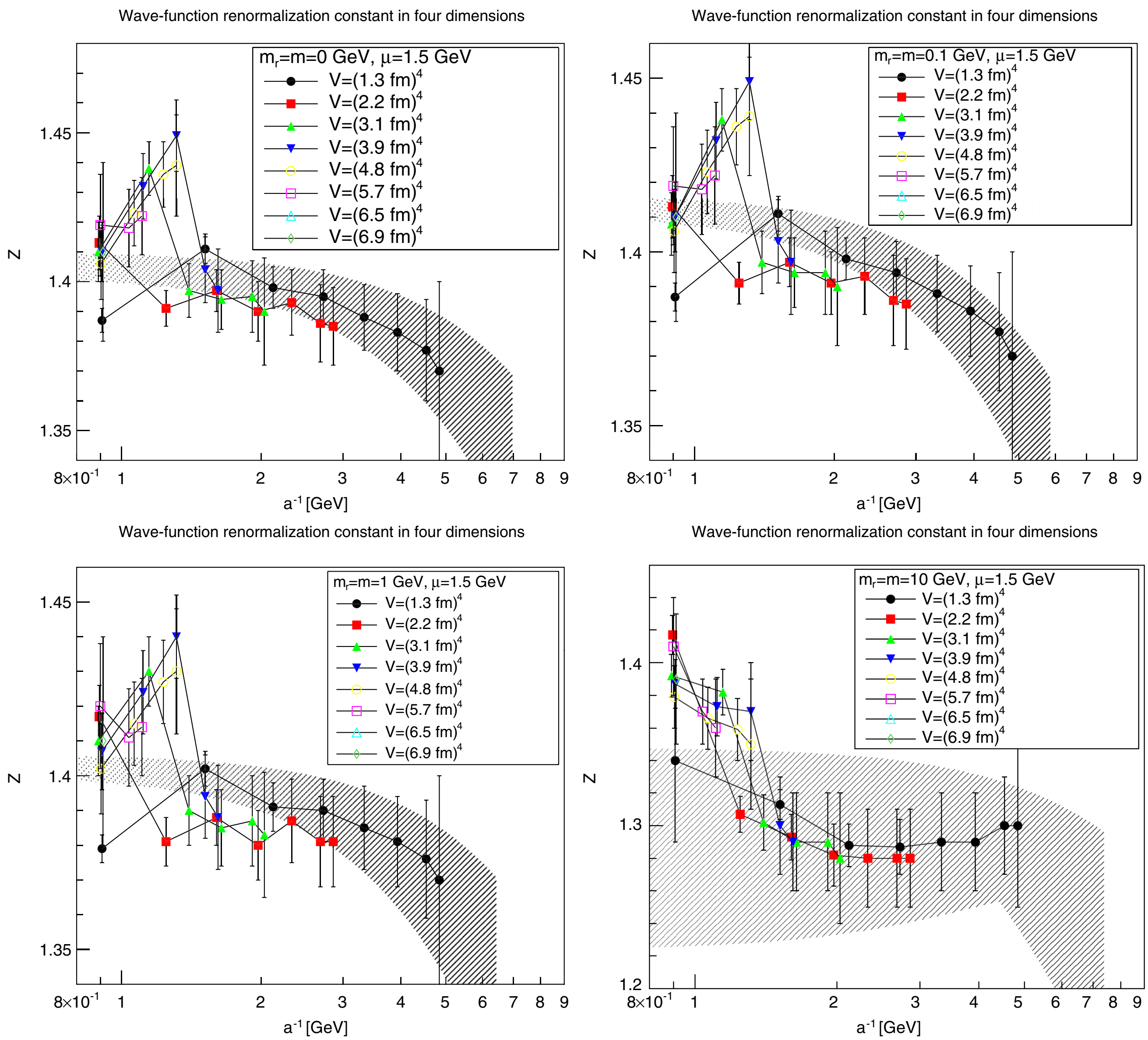

FIG. 5. The wave-function renormalization constant as a function of the lattice cutoff and the lattice volume in four dimensions for $\mu = 1.5$ GeV. The top-left panel shows the case of $m = m_r = 0$ GeV, the top-right panel of $m = m_r = 0.1$ GeV, the bottom-left panel of $m = m_r = 1$ GeV, and the bottom-right panel of $m = m_r = 10$ GeV. The hatched band is the fit (5) with the parameters given in Table I.

in [23,39]. In the continuum, it is given by the inverse of the covariant adjoint Laplacian including the mass term

$$-D^2 = -(\partial_\mu + gf^{abc}A_\mu^c)^2 + m_0^2,$$

where the f^{abc} are the structure constants, for SU(2) just the Levi-Civita tensor, the A_μ^a are the gauge fields, $g = \sqrt{4/\beta}$ the (bare) coupling constant, and m_0 the bare mass of the scalar. As the lattice version of this operator its naive discretization [41]

$$-D_L^2 = -\sum_\mu (U_\mu^a(x)\delta_{y(x+e_\mu)} + U_\mu^{a\dagger}(x-\mu)\delta_{y(x-e_\mu)} - 2\delta_{xy}) + m_0^2\delta_{xy}$$
$$U_{\mu bc}^a = \frac{1}{2}\mathrm{tr}\,(\tau^b U_\mu^\dagger \tau^c U_\mu),$$

has been used, where U_μ^a are the link variables in the adjoint representation and U_μ the usual links in the fundamental representation. The links are transformed between both representations using the generators τ^a, in the present case the Pauli matrices. The e_μ are lattice unit vectors in the corresponding directions. Since this operator is positive semi-definite, it can be inverted. This has been done using the same method as for the Faddeev-Popov operator in [38]. It should be noted that even a zero mass is not a problem for this method.[3] The final result is averaged over color. The momenta are evaluated along the[4] x-axis as edge momenta and along the xy, xyz, and $xyzt$ diagonal directions, when available in a given number of dimensions. This provides access to both the lowest and highest possible momenta for all dimensions with the least corresponding lattice artifacts [32] without employing additional improvements [42,43]. The latter would require again higher statistics at all momenta, e.g., to obtain sufficiently precise renormalization constants for all volumes as well to make effective use of.

Fixing the bare mass m_0 in (1) is done as in [23]: Using the known lattice spacings, it is set to the desired tree-level value $m = am_0$ at the ultraviolet cutoff $1/a$. Four different values will be used, zero, 100 MeV, 1 GeV, and 10 GeV. The bare values m_0 for 1 GeV physical tree-level mass are listed in Table III. In [23], it was found that the lattice artifacts were for all masses comparatively small, even for zero and 10 GeV. As will be seen, this is not the case here, and substantial discretization artifacts are encountered independent of the bare mass. In this respect, adjoint matter is different than fundamental matter.

[3]In contrast to the Faddeev-Popov operator, this operator has no trivial zero modes, and thus an inversion even at zero momentum is possible. However, since constant modes affect the result on a finite lattice, this is not done here, as in [23].

[4]Note that, where possible, the momentum directions are not averaged, as this would require additional expensive inversions but introducing additional correlations.

III. RENORMALIZATION

A. Definition of the renormalization scheme

For the adjoint case, the same scheme will be used as for the fundamental case [23]. For completeness, it will be briefly repeated here. It assumes that the renormalization can be performed as in the perturbative case [44], i.e., a wave-function renormalization constant and a mass renormalization is sufficient. While discretization effects are large it seems that this is indeed possible for sufficiently fine lattices.

There are then two necessary renormalization constants, a multiplicative wave-function renormalization Z, and an additive mass renormalization δm^2. The renormalized propagator is

$$D^{ij}(p^2) = \frac{\delta^{ij}}{Z(p^2 + m_r^2) + \Pi(p^2) + \delta m^2}, \tag{1}$$

where m_r^2 is the renormalized mass, p^2 is the momentum and $\Pi(p^2)$ is the self-energy obtained from the unrenormalized color-averaged propagator $D_u = D_u^{ii}/N_c$,

$$\Pi(p^2) = \frac{1 - p^2 D_u(p^2)}{D_u(p^2)} \tag{2}$$

and, therefore, encodes the deviation from the tree-level propagator

$$D_u = \frac{1}{p^2 + \Pi(p^2)}.$$

The inclusion of the tree-level mass m^2 in the self-energy is technically convenient, as it avoids to use explicitly the scale a.

TABLE I. Fit parameters of (5) for the wave-function renormalization constants in the standard scheme. A value of 0 for Z_∞ indicates that no stable fit with a nonzero value for Z_∞ could be found.

d	m [GeV]	Z_∞	c	Λ [GeV]
2	0	1.116(6)	0.058(1)	4.4(4)
2	0.1	1.118(3)	0.053(6)	4.1(3)
2	1	1.1067(8)	0.0400(14)	1.88(5)
2	10	0.997(3)	0.06401(13)	0.7(1)
3	0	0.847(16)	1.56(5)	5.56(4)
3	0.1	0.85(3)	1.56(12)	5.56(16)
3	1	0.869(5)	1.44(5)	5.58(12)
3	10	1.043(13)	0.176(11)	1.101(6)
4	0	0	7.2(7)	13(4)
4	0.1	0	6.7(5)	11(2)
4	1	0	7.1(8)	12(4)
4	10	0	$6.2^{+1.1}_{-0.9}$	11(4)

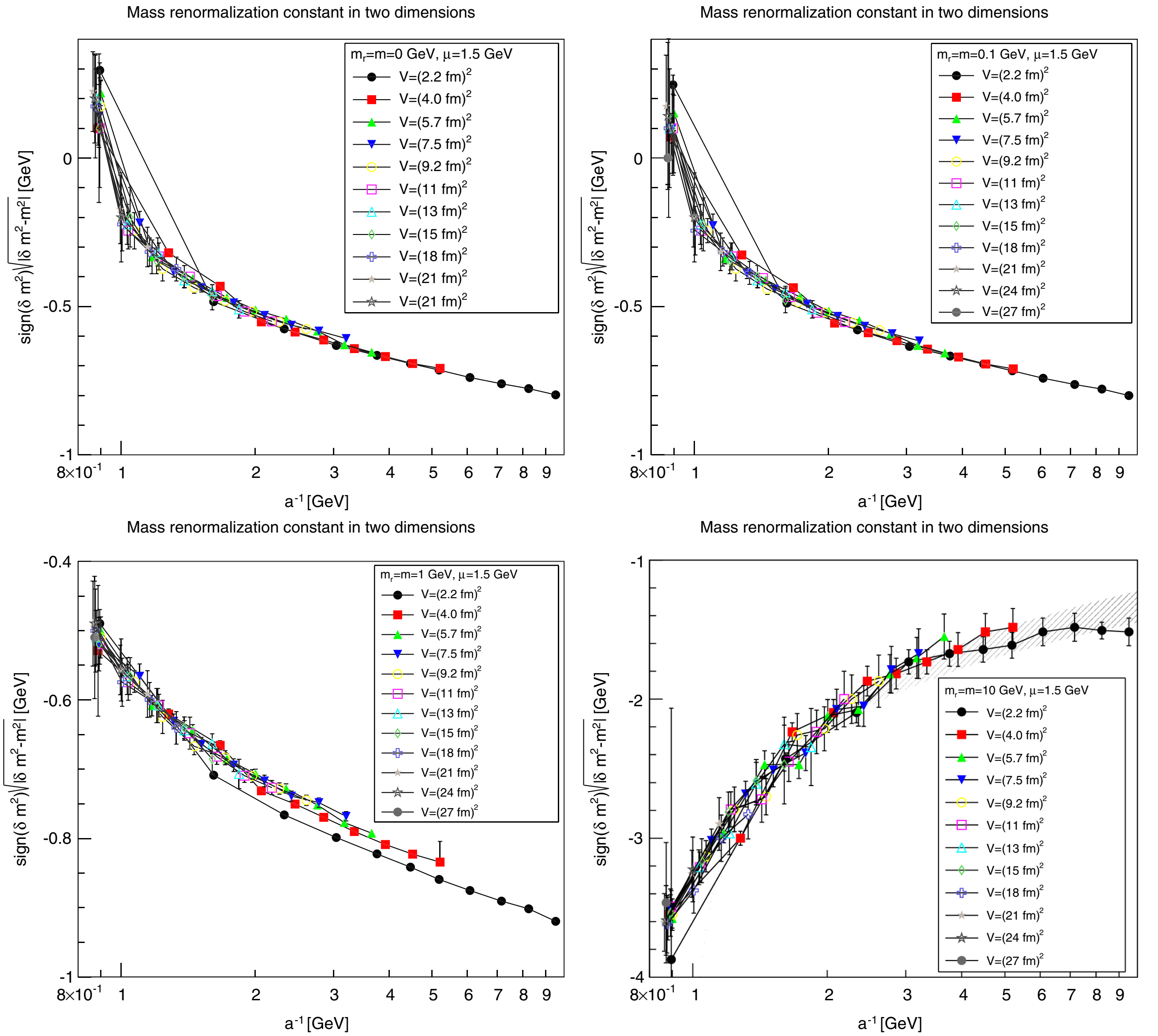

FIG. 6. The mass renormalization constant as a function of the lattice cutoff and the lattice volume in two dimensions for $\mu = 1.5$ GeV. The top-left panel shows the case of $m = m_r = 0$ GeV, the top-right panel of $m = m_r = 0.1$ GeV, the bottom-left panel of $m = m_r = 1$ GeV, and the bottom-right panel of $m = m_r = 10$ GeV. The hatched band is the fit (6) with the parameters given in Table II.

The renormalization scheme is

$$D^{ij}(\mu^2) = \frac{\delta^{ij}}{\mu^2 + m_r^2} \tag{3}$$

$$\frac{\partial D^{ij}}{\partial p}(\mu^2) = -\frac{2\mu\delta^{ij}}{(\mu^2 + m_r^2)^2}$$

$$Z = \frac{2\mu - \frac{d\Pi(p^2)}{dp}(\mu^2)}{2\mu}$$

$$\delta m^2 = \frac{(\mu^2 + m_r^2)\frac{d\Pi(p^2)}{dp}(\mu^2) - 2\mu\Pi(\mu^2)}{2\mu}, \tag{4}$$

with the renormalization scale μ. In most of the paper, the choice $\mu = 1.5$ GeV and $m_r = m$ will be made. The effect of different choices will be investigated in Secs. III C and IV B. Numerically, the constants are determined by linear interpolation between the two momenta values along the x-axis between which the actual value of μ is. The derivative of Π is obtained by deriving the linear interpolation of Π between both points analytically. Errors are determined by error propagation from the statistical bootstrap errors of the propagator [38].

Note that the statistical errors of Z and δm^2 had been propagated back into the renormalized propagator in [23]. This is not done here. The reason is that the mass renormalization δm^2 is found to be very large in comparison

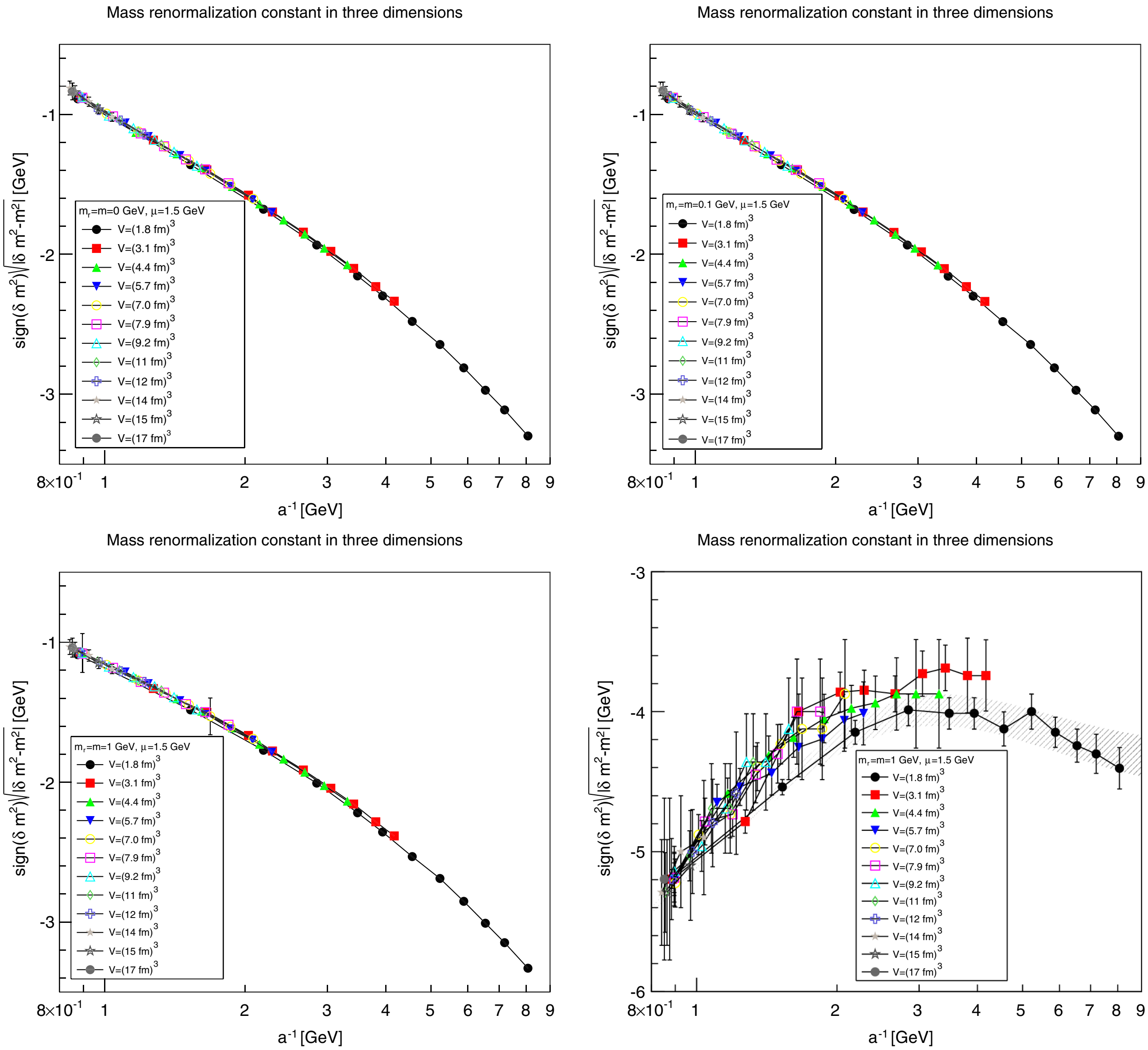

FIG. 7. The mass renormalization constant as a function of the lattice cutoff and the lattice volume in three dimensions for $\mu = 1.5$ GeV. The top-left panel shows the case of $m = m_r = 0$ GeV, the top-right panel of $m = m_r = 0.1$ GeV, the bottom-left panel of $m = m_r = 1$ GeV, and the bottom-right panel of $m = m_r = 10$ GeV. The hatched band is the fit (6) with the parameters given in Table II. Note that the hatched band can be as narrow as the lines, and, therefore, not be visible.

to the fundamental case. If the error is back-propagated, this yielded very large errors, but those were highly correlated, i.e., substantially overestimated the statistical error. This was seen as having almost identical values for different derived quantities, but with error bars much larger than the curves suggest. To avoid this correlation, only the error on Π, determined by error propagation from the only direct lattice measurement of the bare propagator D_u in (2), was propagated into the renormalized propagator (1). That can be equally well seen as defining the renormalization constants, rather than to determine them from the data.

Note that if at the pole location the propagator depends only on $|p|^2$ this is the analytically continued pole scheme. However, as will be seen in Sec. IV, this is not the case in general in the quenched theory.

B. Numerical results and discretization dependence

The effect of renormalization is shown in Fig. 1. It is clearly seen that the unrenormalized propagator depends substantially on a, the more the higher the dimension. This dependency is almost removed by the renormalization prescription of Sec. III A if $a^{-1} \gtrapprox 2$ GeV. Only a slight dependency is left afterwards, decreasing the finer the lattice gets. The residual dependency on a is actually slightly larger the smaller the masses, but the general trend

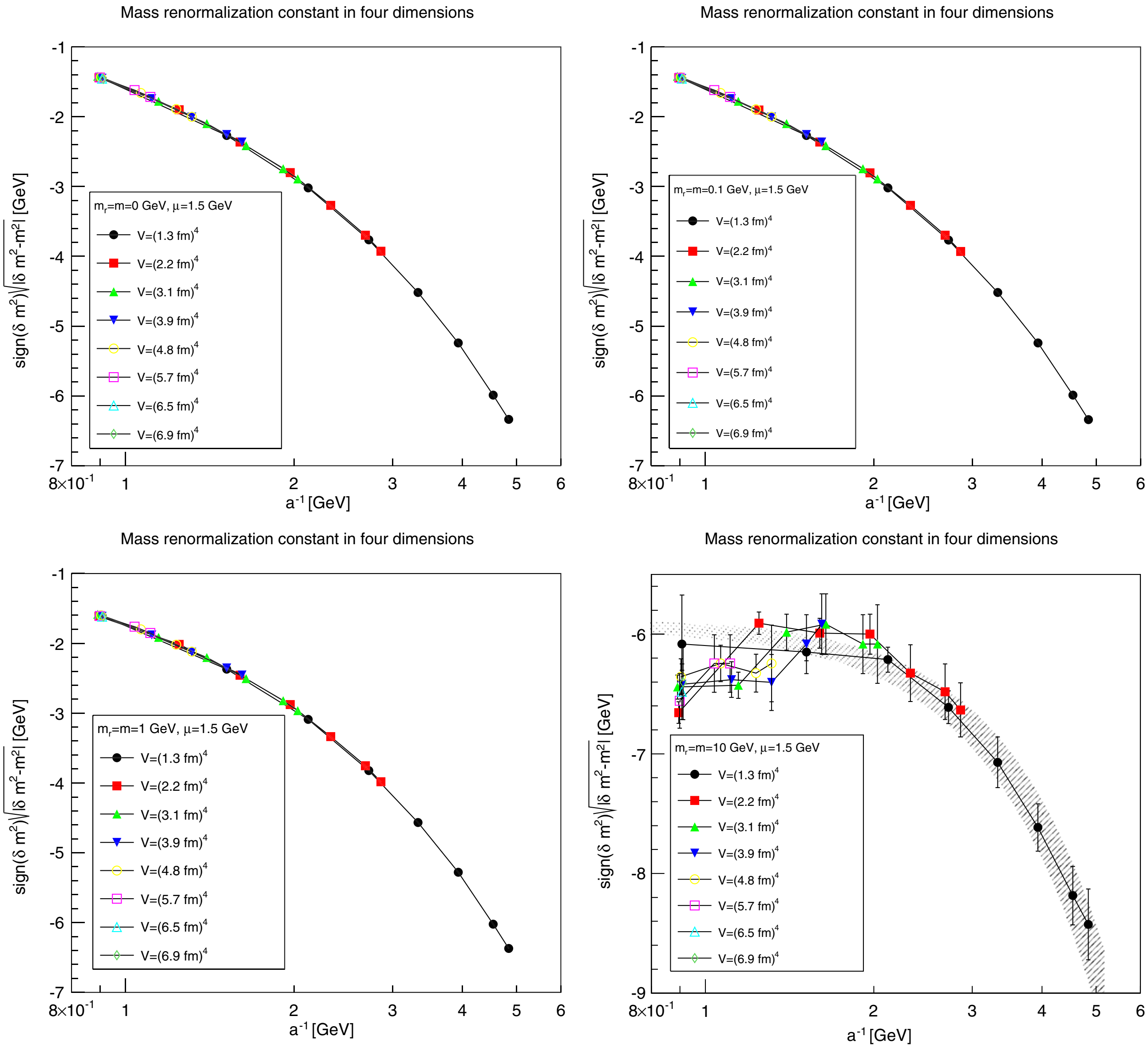

FIG. 8. The mass renormalization constant as a function of the lattice cutoff and the lattice volume in four dimensions for $\mu = 1.5$ GeV. The top-left panel shows the case of $m = m_r = 0$ GeV, the top-right panel of $m = m_r = 0.1$ GeV, the bottom-left panel of $m = m_r = 1$ GeV, and the bottom-right panel of $m = m_r = 10$ GeV. The hatched band is the fit (6) with the parameters given in Table II. Note that the hatched band can be as narrow as the lines, and, therefore, not be visible.

is the same. This is likely also affected by a mixing with finite-volume effects.

Nonetheless, this remainder systematic discretization error is substantially larger than for the fundamental case [23], even though the dependency on a without renormalization is in both cases similar. This will have consequences throughout the rest of the investigation. Therefore, it will be necessary to often assess the volume dependence and a dependence independently, rather than just looking at the finest lattices as it was possible in the fundamental case [23]. To the author, it is not clear where this difference originates from, and will be taken here as an observation which has to be taken into account when judging the results.

Note that, as in the fundamental case [23], the differences mainly arise in the infrared, indicating that the mass renormalization is stronger a dependent than the wave-function renormalization, as expected from perturbation theory. This will be confirmed below in the systematic analysis in Sec. III D.

As in the fundamental case [23] any attempt to improve systematic uncertainties by using more points in the interpolation for the determination of the renormalization constants were more than offset by the increase of the statistical errors. In fact, the statistical fluctuation are found to be stronger for the adjoint case than for the fundamental case. Thus, the linear interpolation described in Sec. III A

TABLE II. Fit parameters of (6) for the mass renormalization constants at $\mu = 1.5$ GeV.

d	m [GeV]	M [GeV]	c [GeV^{3-d}]	Λ [GeV]	ϵ
2	0	−0.138(4)	−0.353(8)	O(10^{-9})	−0.415(9)
2	0.1	−0.160(4)	−0.3348(19)	O(10^{-7})	−0.428(5)
2	1	−0.570(2)	−0.1427(11)	O(10^{-8})	−0.591(5)
2	10	−16(2)	1.18(17)	O(10^{-4})	0.008(3)
3	0	−0.4117(4)	−1.489(5)	3.055(19)	0.973(3)
3	0.1	−0.42(5)	−1.50(3)	3.09(12)	0.978(5)
3	1	−0.670(3)	−1.259(6)	3.266(14)	0.912(3)
3	10	−6.9(3)	18.8(13)	3.1(1)	2.79(15)
4	0	−1.092(11)	−2.25(7)	2.59(5)	1.88(3)
4	0.1	−1.094(11)	−2.26(7)	2.59(5)	1.88(3)
4	1	−1.283(6)	−2.20(7)	2.71(5)	1.88(3)
4	10	−5.93(5)	−0.065(12)	0.95(5)	−0.48(8)

will be used throughout. Still, in cases where the renormalization point is mainly dominated by a single of the two points in the interpolation this can induce an additional systematic error, as is seen, e.g., at $a^{-1} = 1.14$ GeV in four dimensions in Fig. 1. This case will happen less and less the closer the lattice parameters are to the thermodynamic limit.

C. Scale and scheme dependence

Of course, the choice of scheme in Sec. III A is completely arbitrary. To test the impact of this choice on the propagator in momentum space both the renormalized mass and the renormalization scale will be varied. However, this can give only then a reasonable estimate of the effects if

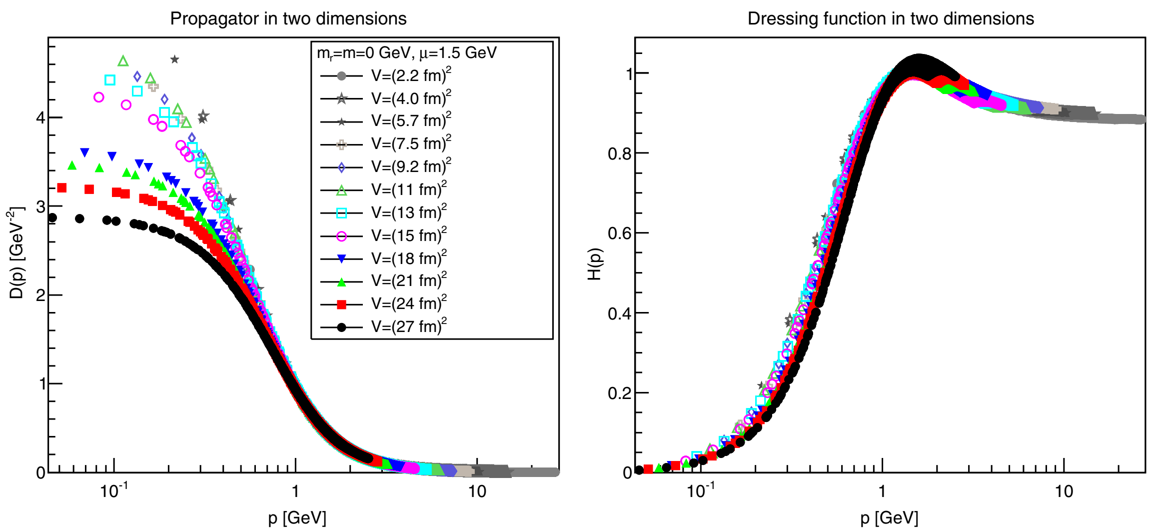

FIG. 9. The propagator (left panel) and the dressing function (7) (right panel) in two dimensions for $m = m_r = 0$ GeV and $\mu = 1.5$ GeV.

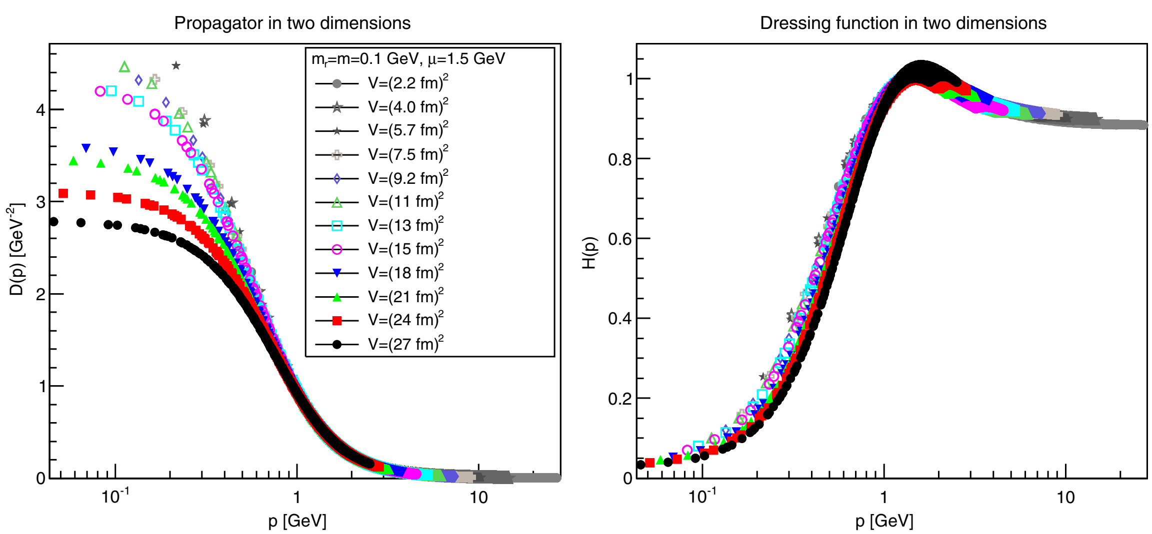

FIG. 10. The propagator (left panel) and the dressing function (7) (right panel) in two dimensions for $m = m_r = 0.1$ GeV and $\mu = 1.5$ GeV.

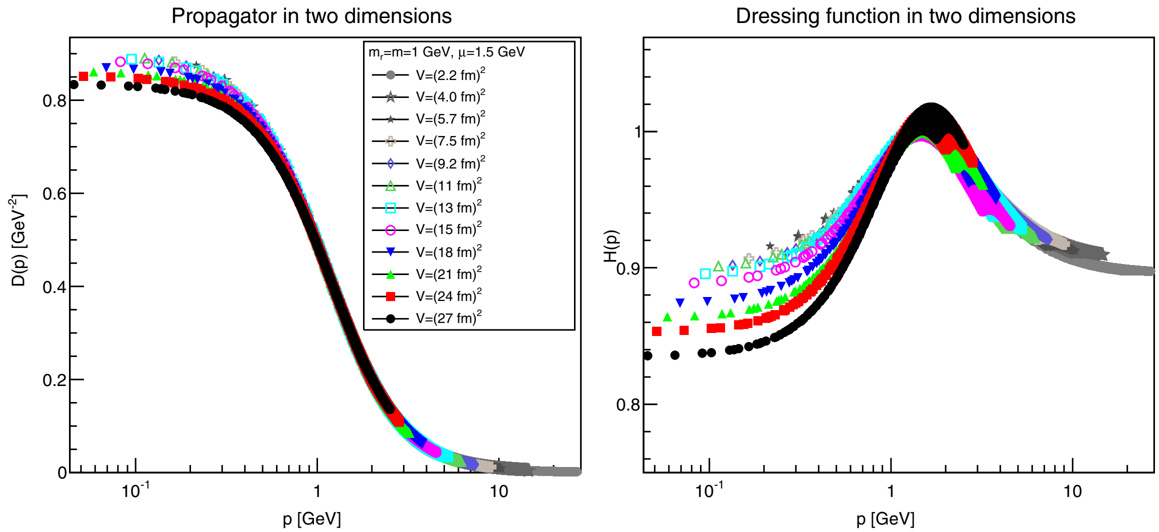

FIG. 11. The propagator (left panel) and the dressing function (7) (right panel) in two dimensions for $m = m_r = 1$ GeV and $\mu = 1.5$ GeV. Note the different scale in the right-hand panel compared to Figs. 9 and 10.

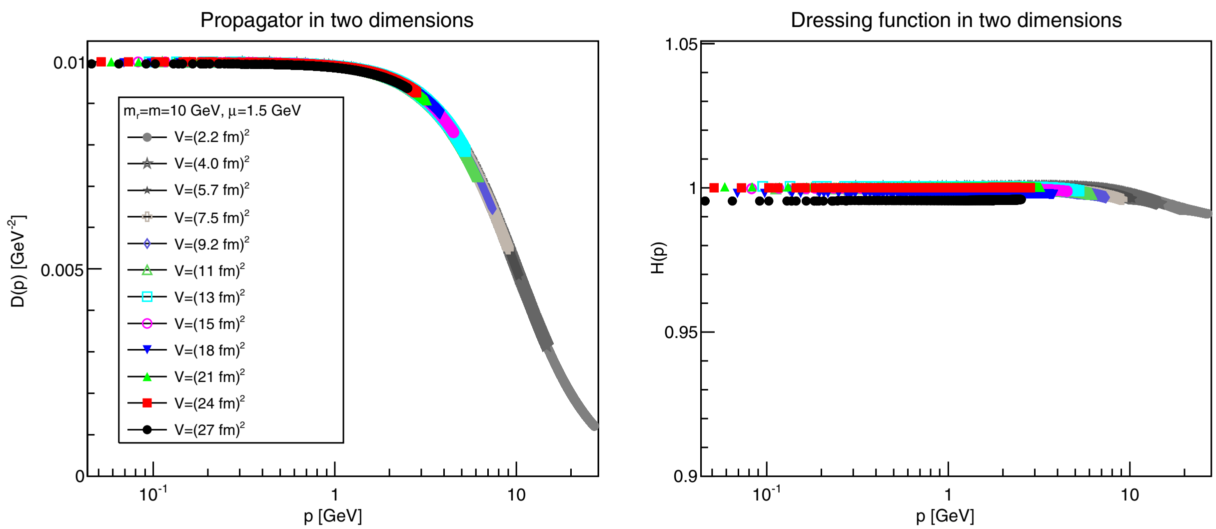

FIG. 12. The propagator (left panel) and the dressing function (7) (right panel) in two dimensions for $m = m_r = 10$ GeV and $\mu = 1.5$ GeV. Note the different scale in the right-hand panel compared to Figs. 9 and 10.

the range is not probing the extremes of the lattice, requiring a sufficiently fine resolution. Also, the bare mass should be sufficiently far away from the extremes of the lattice. Thus, in the following the case $m = 1$ GeV will be considered, requiring volumes for which lattice spacings $a^{-1} \gtrsim (2\ \mathrm{GeV})^{-1}$ are available. Furthermore, for the sake of comparability the same physical volumes will be used as in [23].

The results are shown for both scale and scheme dependence in Fig. 2. The dependence on the scale is relatively mild. Because of the derivative condition (4), the change of scale leads to a tilting of the propagator, due to its monotonous behavior. That the strongest effect is seen in the infrared indicates already that the largest deviation from tree-level will be encountered there. This is also emphasized by the scheme dependence. When introducing a large mass scale by the renormalization a closer resemblance to tree-level is obtained. However, if introducing a smaller mass scale larger deviations are seen. It appears that there is an intrinsic mass-scale, similar to the fundamental case [23], which adds to the mass scale introduced by the scheme. This will be investigated, and confirmed, further in Sec. IV. At any rate, there is little difference between the different dimensionalities.

D. Dependence of the renormalization constants on the volume and the cutoff

For unquenched simulations [21] it is much harder to find lines-of-constant physics. In addition, investigating multiple

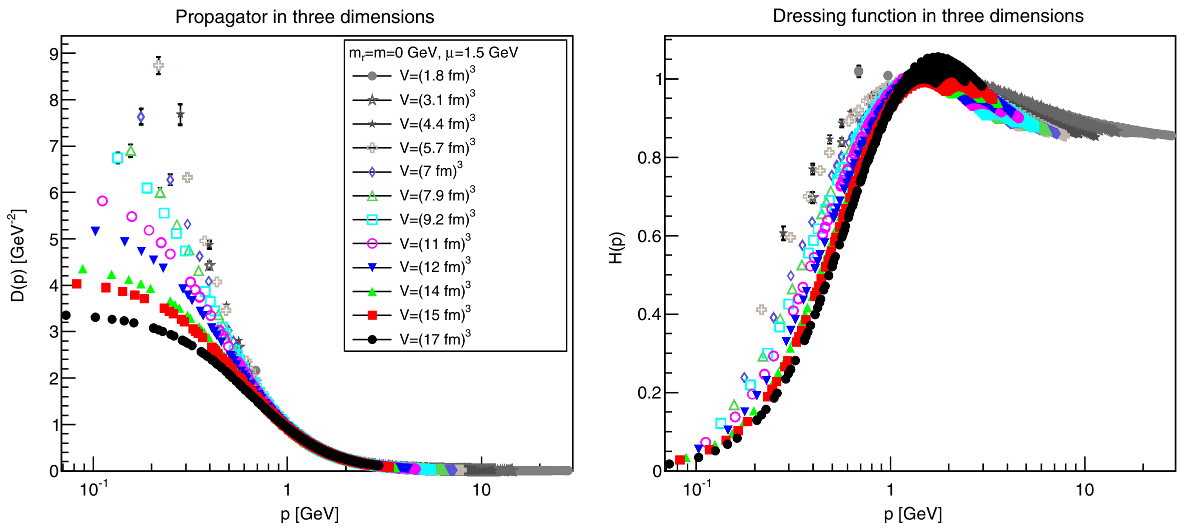

FIG. 13. The propagator (left panel) and the dressing function (7) (right panel) in three dimensions for $m = m_r = 0$ GeV and $\mu = 1.5$ GeV.

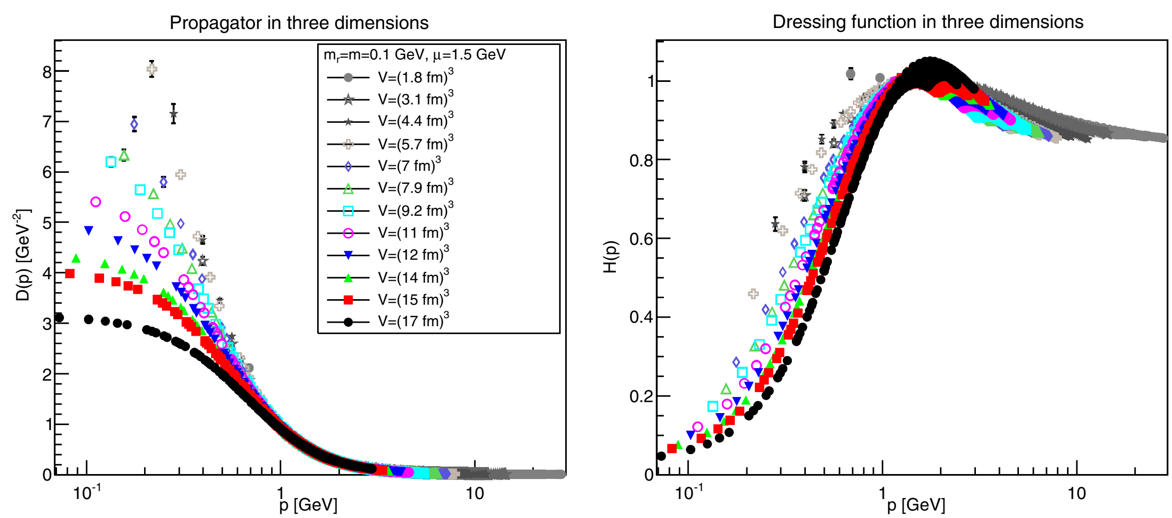

FIG. 14. The propagator (left panel) and the dressing function (7) (right panel) in three dimensions for $m = m_r = 0.1$ GeV and $\mu = 1.5$ GeV.

volumes is expensive due to the amount of configurations necessary for spectroscopy. Hence, it is quite important to know how renormalization needs to be performed as a function of lattice parameters, and how it is influenced by discretization and finite-volume artifacts. For the fundamental case [23], it was found that the functional dependence on a^{-1} was of the qualitative form expected from perturbation theory [44], and a dependence on volume was quasi nonexistent, even for rather small volumes. This permits to obtain high-precision renormalization constants on small volumes to be used on larger volumes. It will be seen that the same is true for the adjoint case. Note that in the following only the standard scheme $m_r = m$ with a renormalization scale $\mu = 1.5$ GeV will be investigated. In other schemes, this finding could not be true.

The wave-function renormalization is shown in Figs. 3–5 for varying dimensionalities. In all cases, it decreases eventually with increasing $1/a$. There is some finite-volume dependence visible, especially in three dimensions. However, this seems to be essentially only a rescaling, as for the fundamental case [23]. The qualitative behavior seems to be volume independent. There is also a jumping behavior in four dimensions when a^{-1} crosses a critical, volume-dependent value. This hints to a mass-scale, which increases with increasing volume, which has to be crossed before the asymptotic behavior can be reached. Indeed, there is a mass scale different from the renormalized mass present, as will be discussed in Sec. IV.

It is, therefore, useful to investigate the asymptotic behavior at large cutoffs, thus utilizing the smallest volume.

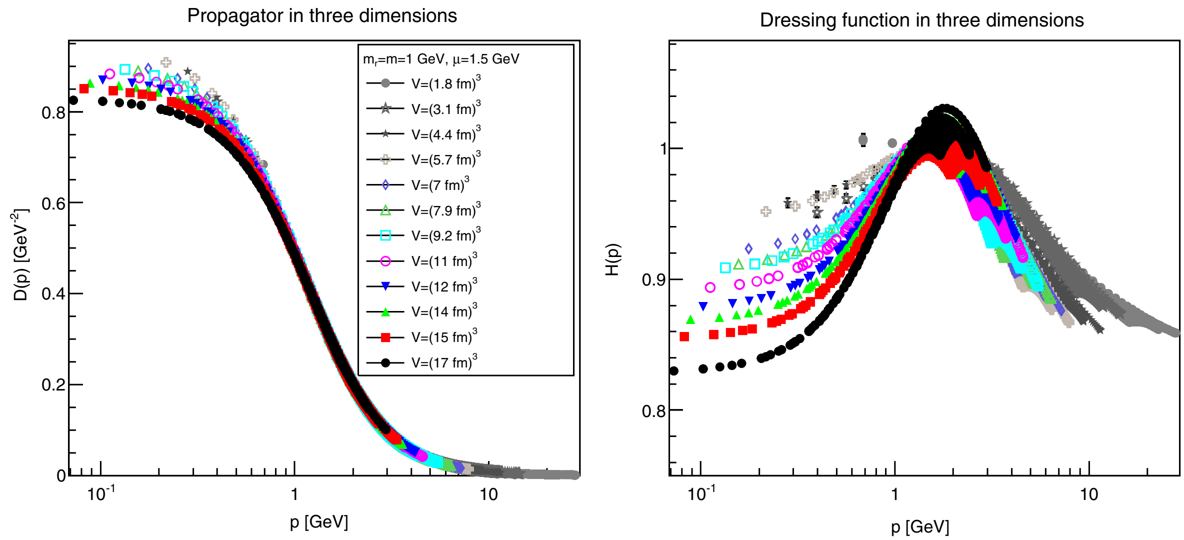

FIG. 15. The propagator (left panel) and the dressing function (7) (right panel) in three dimensions for $m = m_r = 1$ GeV and $\mu = 1.5$ GeV. Note the different scale in the right-hand panel compared to Figs. 13 and 14.

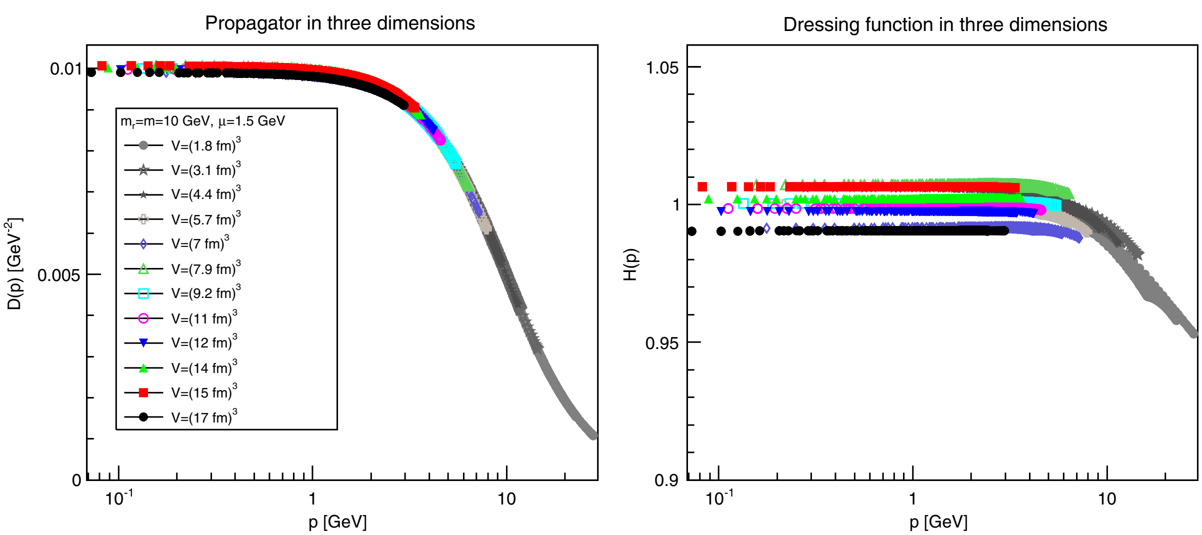

FIG. 16. The propagator (left panel) and the dressing function (7) (right panel) in three dimensions for $m = m_r = 10$ GeV and $\mu = 1.5$ GeV. Note the different scale in the right-hand panel compared to Figs. 13 and 14.

The slow evolution and the fundamental case [23] suggest a logarithmic behavior. Indeed, an ansatz

$$Z(a) = Z_\infty + \frac{b}{\ln\left(\frac{a^{-2}+\Lambda^2}{(1\text{ GeV})^2}\right)} \tag{5}$$

provides a reasonable good approximation, as is visible in Figs. 3–5. The fit parameters can be found in Table I.

There are two interesting observations. The first is that, in four dimensions, Z_∞ is zero, while it is nonzero in lower dimensions, in agreement with perturbative expectations [44]. Incidentally, this already hints that the adjoint scalar is not a physical particle, due to the Oehme-Zimmermann superconvergence relation [45]. It is also the same pattern as in the fundamental case [23].

The second is that the fit parameters become increasingly mass independent the higher the dimension. In particular, within errors, they are completely mass independent in four dimensions. This is the more remarkable as a^{-1} is in four dimensions at most of the order of the largest mass. Interestingly, also the scale Λ is quite large, much larger than in the fundamental case [23], where it is essentially 1 GeV. This is in-line with results from the fermion sector [13,24] as well as from glueball masses [46] which suggest an intrinsically higher value for adjoint scales than for fundamental scales.

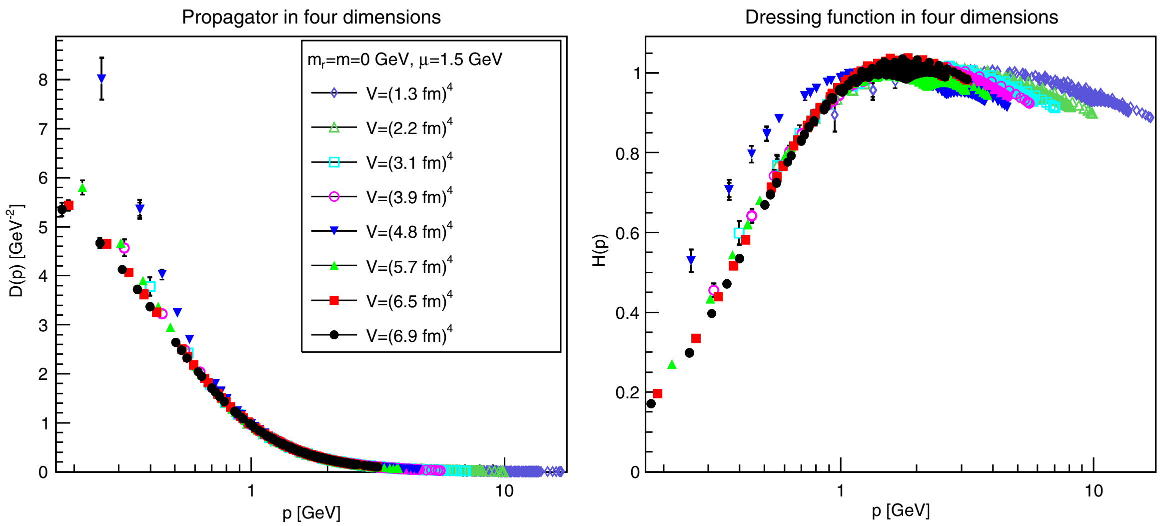

FIG. 17. The propagator (left panel) and the dressing function (7) (right panel) in four dimensions for $m = m_r = 0$ GeV and $\mu = 1.5$ GeV.

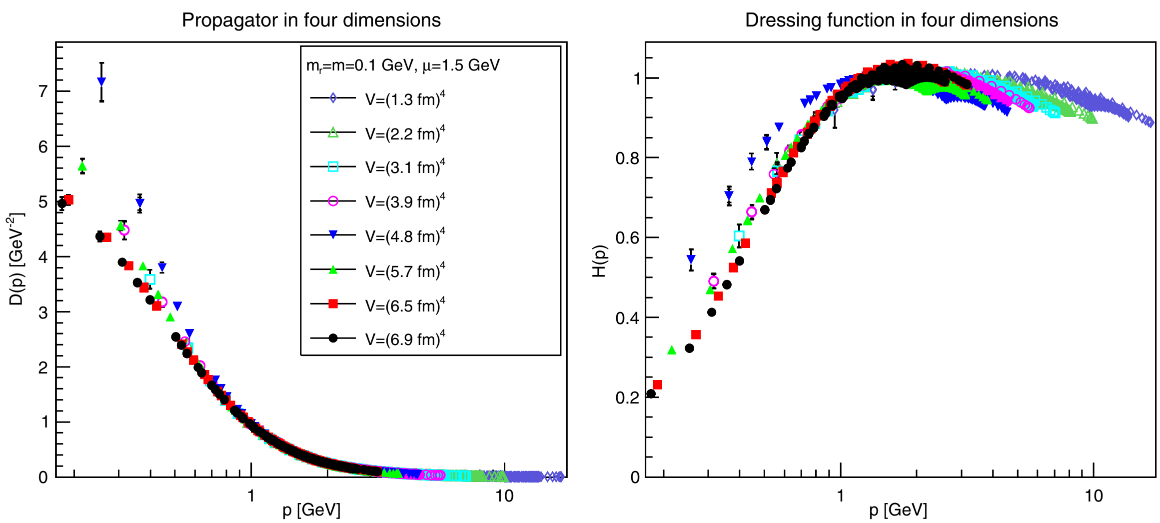

FIG. 18. The propagator (left panel) and the dressing function (7) (right panel) in four dimensions for $m = m_r = 0.1$ GeV and $\mu = 1.5$ GeV.

The situation for the mass renormalization constant, more precisely for $(|\delta m^2 - m^2|)^{1/2}$, is shown in Figs. 6–8.

The results can be fitted rather well by the form

$$\delta m^2(a) - m^2 = -\left(M + ca^{2-d}\left(\ln\left(\frac{\Lambda^2 + a^{-2}}{(1\ \mathrm{GeV})^2}\right)\right)^{\epsilon}\right)^2. \tag{6}$$

The fit parameters are listed in Table II. As expected, the dependence on a^{-1} is purely logarithmic in two dimensions, linear in three dimensions, and quadratic in four dimensions. In the latter cases, also, logarithmic corrections appear, as expected [44,47]. The logarithms also exhibit anomalous dimensions. In general, except in two dimensions and aside from M, the fit parameters are almost independent of the bare mass. Only for the largest bare mass this is not true, but this is conceivably a discretization artifact. In fact, the a dependence in the latter case is different at small $1/a$, but at large $1/a$ the behavior starts to change and to become similar to the ones at smaller bare mass. This behavior is once more similar to the fundamental case [23].[5] Hence, the asymptotic behavior seems to emerge only for $a^{-1} \gtrsim m$.

[5]Note that for the fundamental case it was possible to fit the leading a dependence in (6), rather than to set it to $2 - d$. This did not yield stable fits in the present case, and, therefore, this behavior was fixed.

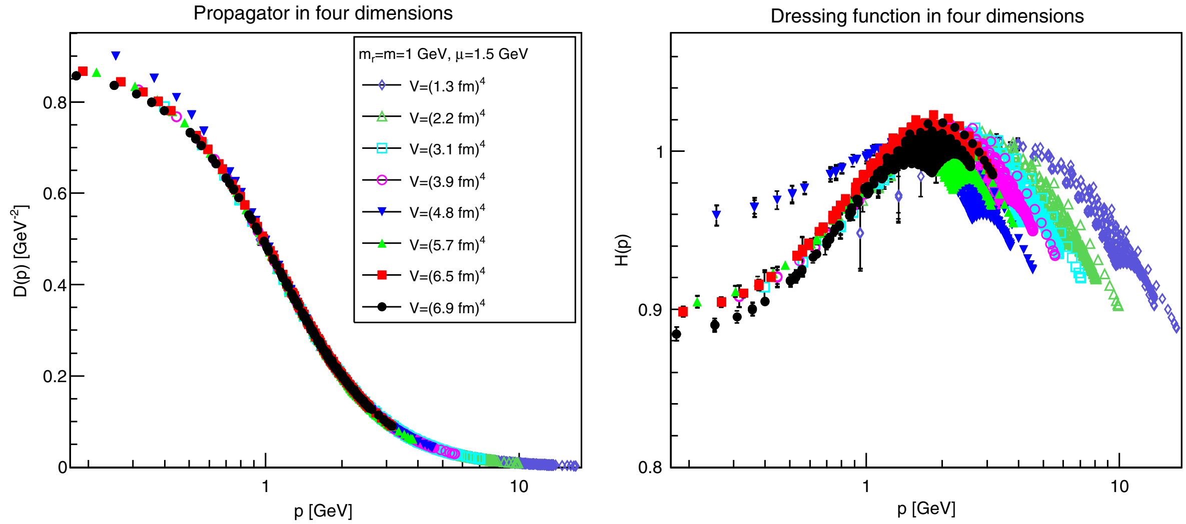

FIG. 19. The propagator (left panel) and the dressing function (7) (right panel) in four dimensions for $m = m_r = 1$ GeV and $\mu = 1.5$ GeV. Note the different scale in the right-hand panel compared to Figs. 17 and 18.

Interestingly, the only parameter showing a pronounced dependence on the mass is $-M$. It behaves roughly like constant $+ m/d$, with the characteristic constant being roughly 0.15, 0.4, and 1 GeV in two, three, and four dimensions, respectively. This once more indicates an intrinsic scale.

IV. ANALYTIC STRUCTURE

A. Momentum-space properties

The results of the previous section, especially Fig. 1, suggest that discretization artifacts are sizable, particularly in the infrared. Thus, in the following not only the results for the finest lattices but also at fixed a^{-1} will be considered.

In addition to the propagator, the dressing function, defined as

$$H(p^2) = (p^2 + m_r^2)D(p^2), \tag{7}$$

will also be presented. The dressing function, therefore, describes the deviation from the (renormalized) tree-level form. By construction at μ all dressing functions equal 1.

The results are shown for two dimensions in Figs. 9–12, for three dimensions in Figs. 13–16, and for four dimensions in Figs. 17–20. From the dressing functions at large momenta, substantial discretization artifacts are visible. They lead to a deviation away from the continuum limit, especially in four dimensions. This is quite similar in kind

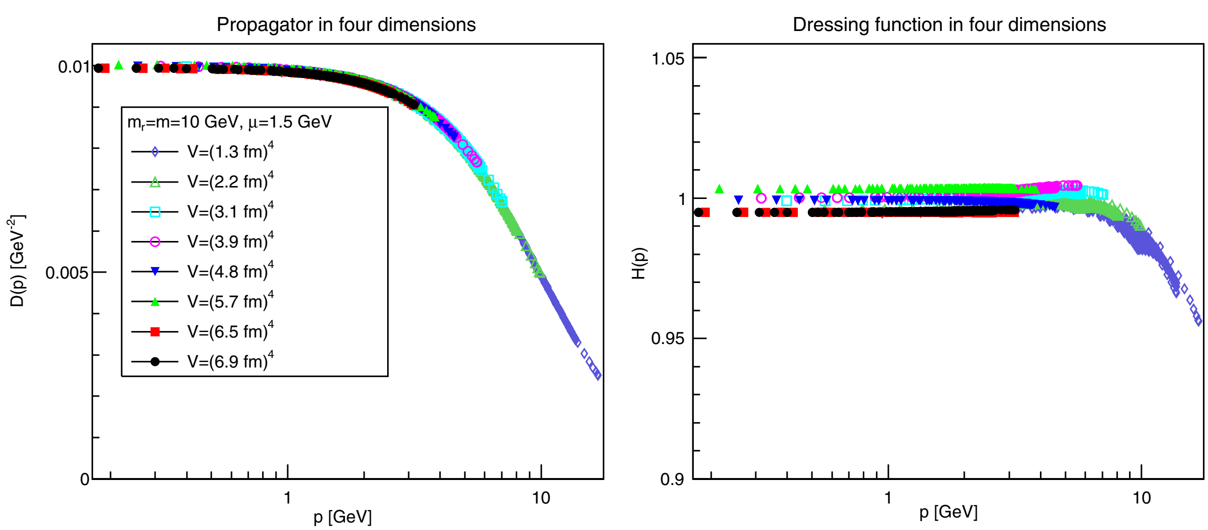

FIG. 20. The propagator (left panel) and the dressing function (7) (right panel) in four dimensions for $m = m_r = 10$ GeV and $\mu = 1.5$ GeV. Note the different scale in the right-hand panel compared to Figs. 17 and 18.

to the other propagators [32] and could be improved using the techniques described, e.g., in [42,43].

At low momenta, a marked infrared suppression compared to the renormalized tree-level behavior is visible from the propagators. This is the stronger the smaller m. Only for $m = m_r = 10$ GeV (almost) no such effect is seen. A similar effect was also observed for the fundamental case [23], but it is much stronger here, suggesting a much larger screening effect. A stronger screening in the adjoint case than in the fundamental case is also observed

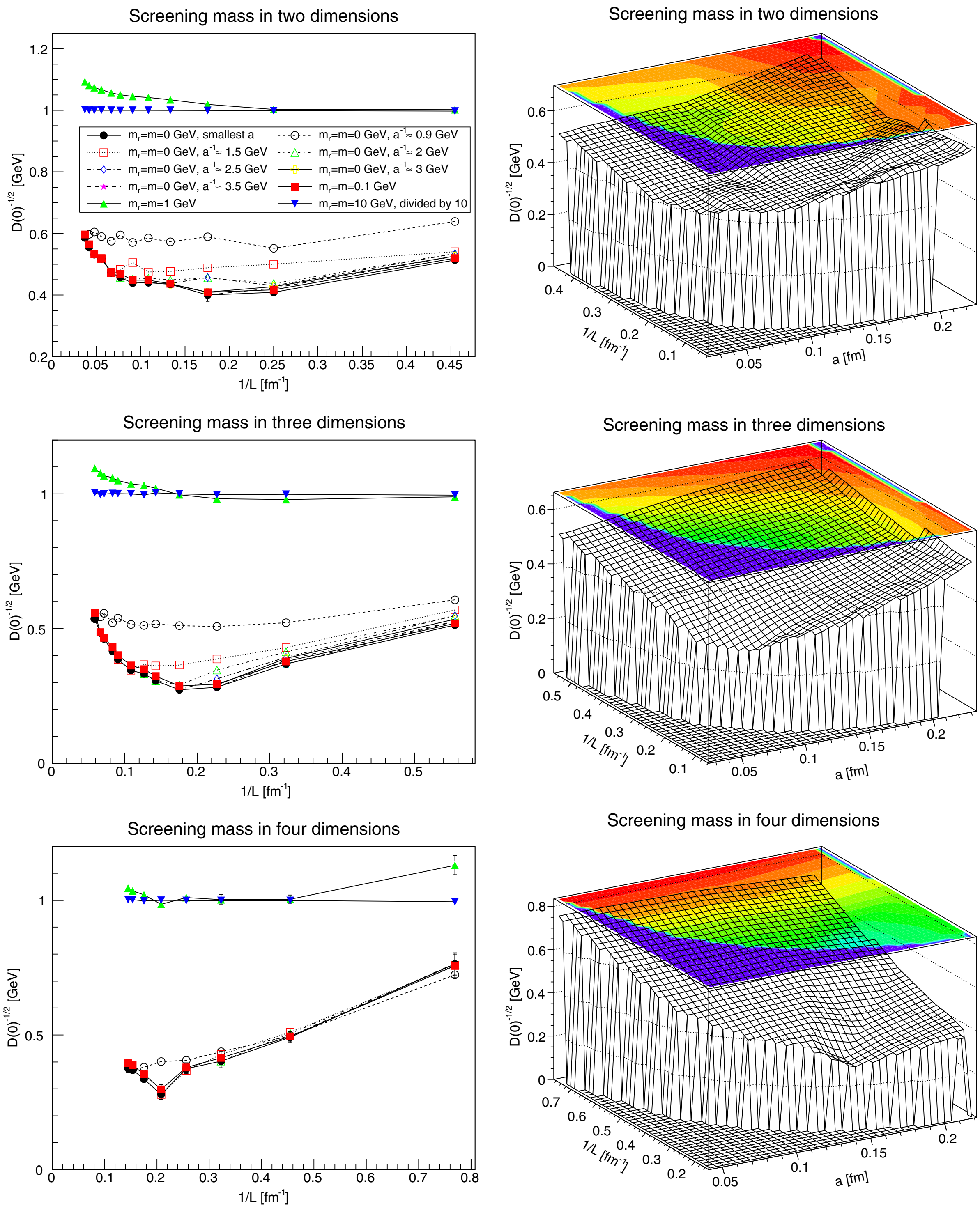

FIG. 21. The value of the screening mass $D(0)^{-1/2}$ as a function of lattice extent in two (top panel), three (middle panel), and four dimensions (bottom panel). The various dashed lines show the dependence at roughly fixed a. The right-hand-side is at $m_r = m = 0$.

for fermions [2,8,11–13]. In addition, there are stronger finite-volume effects than in the fundamental case, especially at low m. They, therefore, extend to larger momenta, up to a few hundred MeV. However, this is intertwined with the discretization artifacts.

To study the combination of both effects in more detail, in Fig. 21 the screening mass $D(0)^{-1/2}$ is shown as a function of physical lattice extension and discretization. Note that since the propagator has not been evaluated at zero momentum, this value is obtained by a linear extrapolation of the propagator at the two lowest nonzero momenta. There is a quite different trend than in the fundamental case [23]. There, after some initial effects, the screening mass became essentially volume independent.

The situation here in the adjoint case is quite different. It is also quite different for the different numbers of dimensions. In two dimensions, there is, except for the coarsest lattices, little dependency on volume at fixed lattice spacing. But there is a pronounced dependency on the lattice spacing at fixed volume. Still, The results tend visibly towards a finite value of about 400–500 MeV in the continuum limit. The situation is far less obvious in three dimensions. There a pronounced dependency on both the lattice spacing and the physical lattice extension is seen. It is not yet sure that the screening mass tends towards a finite value in the thermodynamic limit. However, for the finest and largest lattices the value is still at about 300 MeV, and thus of comparable size to the one in two dimensions. If it would vanish, it would need to do so substantially faster than linear. In four dimensions, the situation changes once more. Now the results are much less dependent on the discretization, but show a strong dependency on the physical volume, reaching down again to values of about 300 MeV. Once more, it is not clear if it surely extrapolates

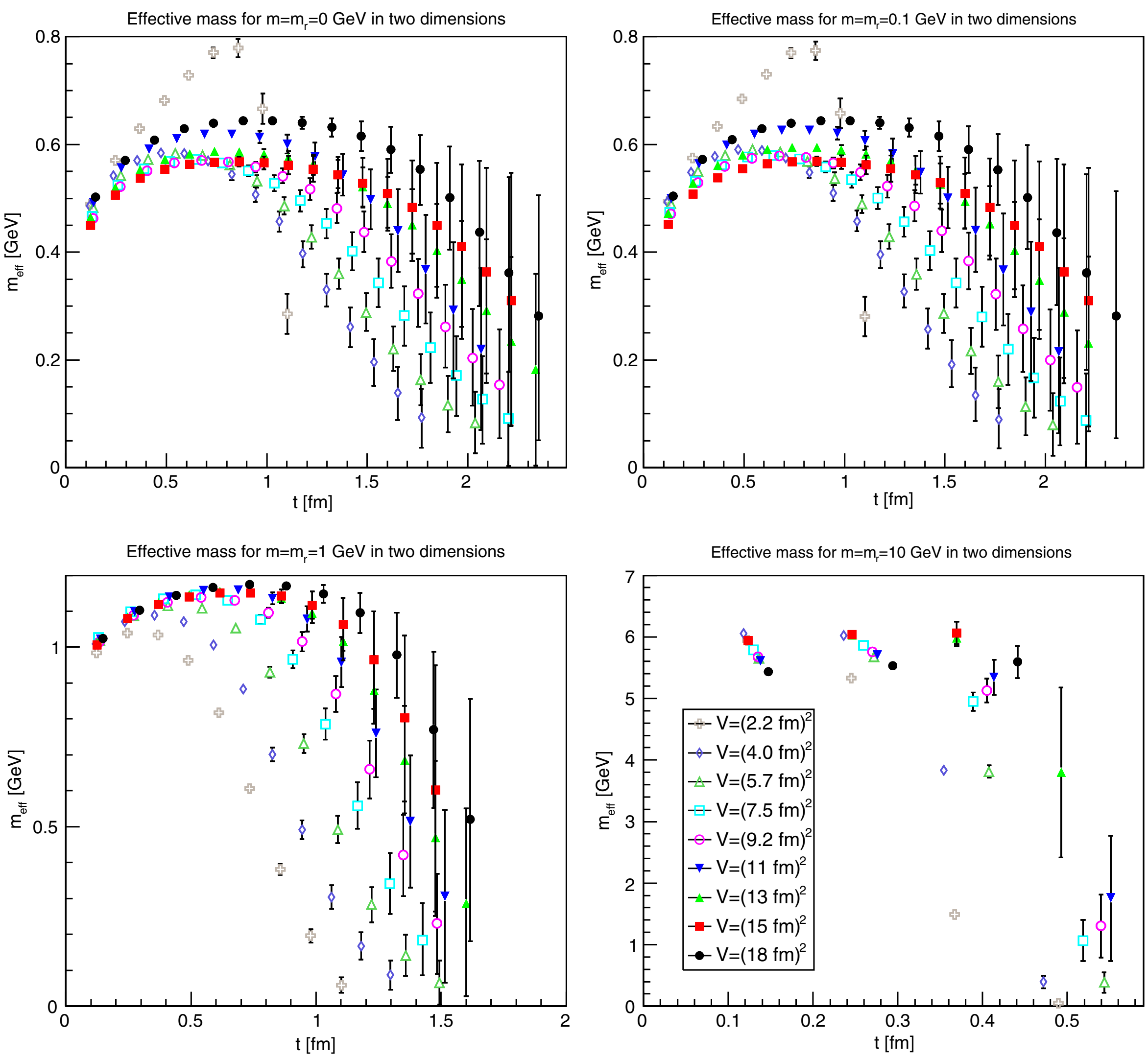

FIG. 22. The effective mass (8) in two dimensions at lattice spacing $a^{-1} \approx 1.5$ GeV. The top-left panel shows the case of $m = m_r = 0$ GeV, the top-right panel of $m = m_r = 0.1$ GeV, the bottom-left panel of $m = m_r = 1$ GeV, and the bottom-right panel of $m = m_r = 10$ GeV. Points with more than 100% relative error are suppressed.

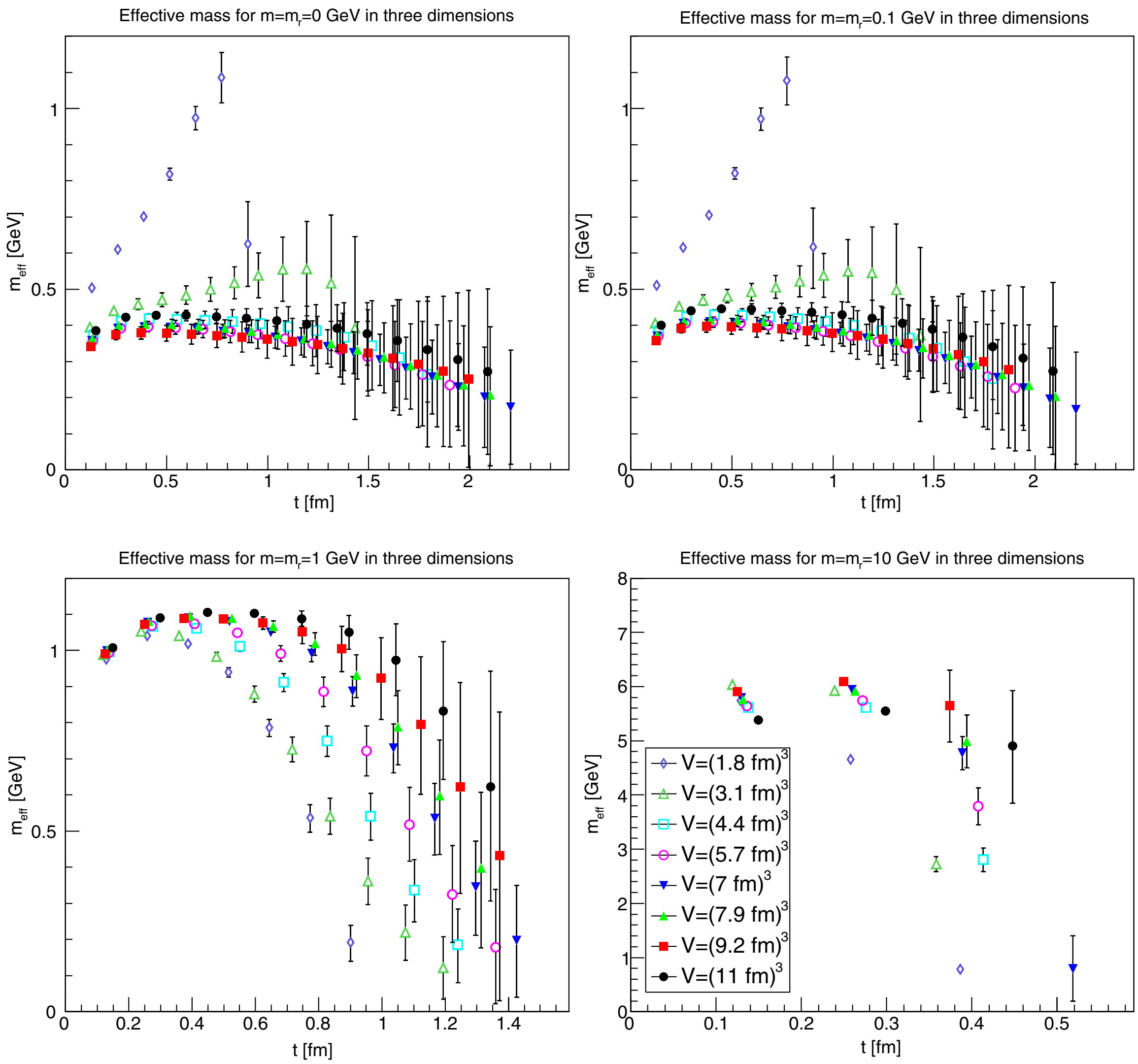

FIG. 23. The effective mass (8) in three dimensions at lattice spacing $a^{-1} \approx 1.5$ GeV. The top-left panel shows the case of $m = m_r = 0$ GeV, the top-right panel of $m = m_r = 0.1$ GeV, the bottom-left panel of $m = m_r = 1$ GeV, and the bottom-right panel of $m = m_r = 10$ GeV. Points with more than 100% relative error are suppressed.

to a nonzero value in the thermodynamic limit, but again if it vanishes it needs to do so much faster than linear.

Note that the trends are also surprisingly true for the large tree-level mass of 1 GeV, though here the effect is much weaker than for the lighter tree-level masses. Still, this indicates a screening which intensifies with larger volumes, while it was, more or less, constant in the fundamental case. In particular, the screening mass is substantially larger than zero, even for the case of zero tree-level and renormalized mass. The size of this screening mass in the massless case of 300–500 MeV for the largest volume is somewhat larger than in the fundamental case, where it was of order 200–250 MeV. The same effect is also seen for adjoint quarks in comparison to fundamental quarks: The effective screening mass for the adjoint quarks is much larger than for the fundamental ones, almost a factor of three [13,24–26]. In this sense, the situation for the adjoint scalars is less drastic.

At larger momenta the behavior is far less drastic. As seen in Figs. 9–20 the propagators follow at higher momenta more or less the expected pattern. At momenta much larger than the renormalization scale the propagators start again to deviate from the tree-level one. In four dimensions, this follows from the usual logarithmic running. In lower dimensions, this is somewhat unexpected, and in contrast to the gauge propagators [3]. This is, however, likely due to the additional wave-function renormalization, which compensates partly for a self-energy contribution, and this discrepancy yields the observed effect: Due to asymptotic freedom, at large momenta all propagators in two and three dimensions tend to $D = 1/(Zp^2)$, yielding $H(p) = 1/Z$, rather than unity.

In addition, in lower dimensions also, additional logarithmic corrections can arise on top of the usual power law [47], which could potentially also contribute.

B. Schwinger function and effective mass

The Schwinger function

$$\Delta(t) = \frac{1}{\pi}\int_0^\infty dp_0 \cos(tp_0) D(p_0^2)$$
$$= \frac{1}{a\pi}\frac{1}{N_t}\sum_{P_0=0}^{N_t-1}\cos\left(\frac{2\pi t P_0}{N_t}\right) D(P_0^2),$$

essentially the temporal correlator, is obtained from the renormalized propagator. The calculation is straightforward in principle, though requires obtaining the removed value at zero momentum. As above, this is obtained by a linear extrapolation of the propagator at the two lowest momenta. Because of the relatively large statistical noise, this induces a corresponding larger error. Systematically, any uncertainty in this constant will vanish as a function of the physical volume, as the extrapolation is done over a smaller and smaller distance in momentum. It can, therefore, be considered an additional finite-volume effect.

From the Schwinger function, the effective (time-dependent) mass

$$m_{\text{eff}}(t) = -\ln\frac{\Delta(t+a)}{\Delta(t)}, \tag{8}$$

can be derived. If the Schwinger function decays strictly like an exponential, this mass will be time independent and

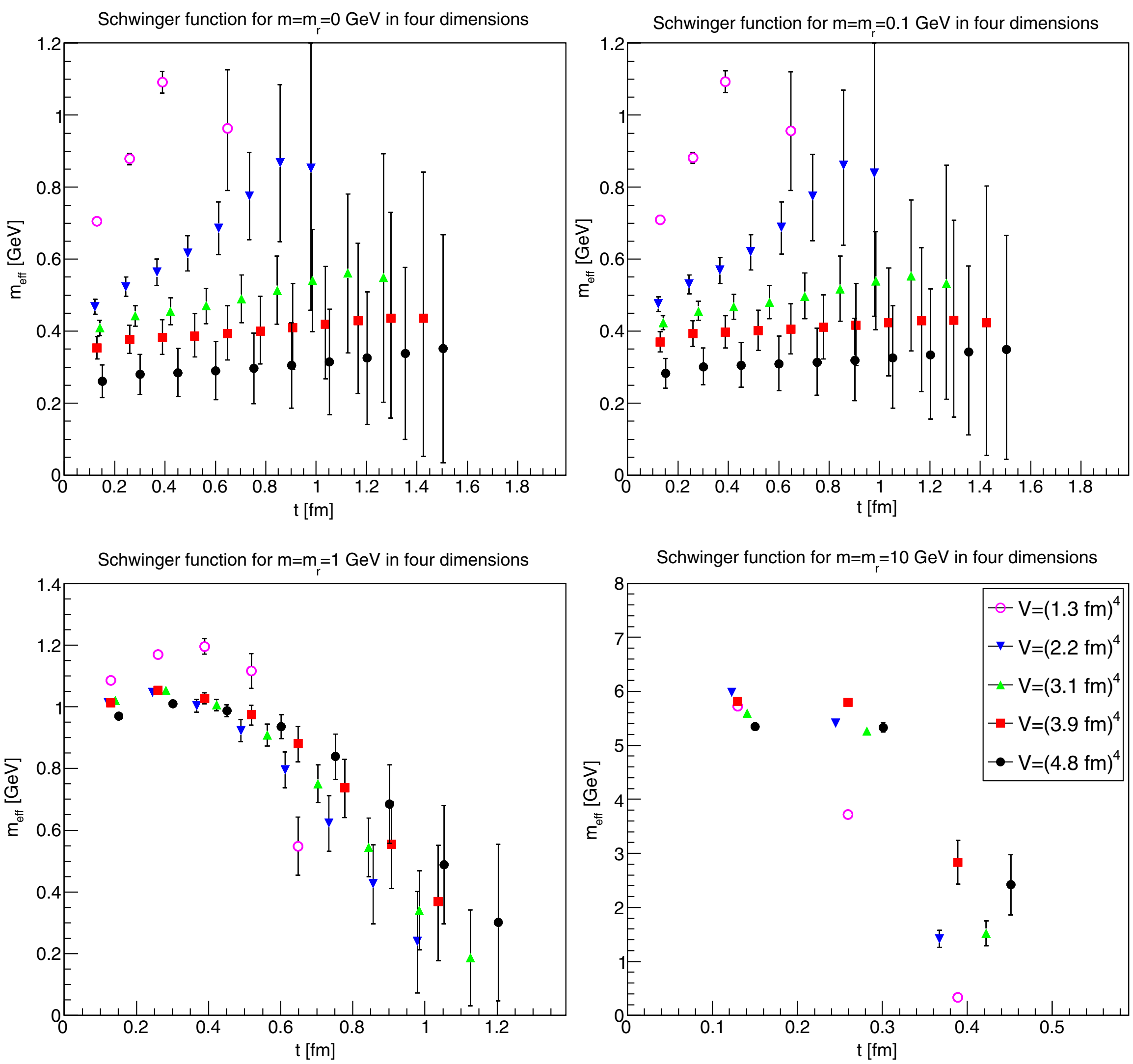

FIG. 24. The effective mass (8) in four dimensions at lattice spacing $a^{-1} \approx 1.5$ GeV. The top-left panel shows the case of $m = m_r = 0$ GeV, the top-right panel of $m = m_r = 0.1$ GeV, the bottom-left panel of $m = m_r = 1$ GeV, and the bottom-right panel of $m = m_r = 10$ GeV. Points with more than 100% relative error are suppressed.

coincide with the pole mass [48]. On a finite lattice, for any physical particle with a positive spectral function, this effective mass is a monotonously decreasing function for $t \leq L/2$. Eventually, at sufficiently long time, it is just the energy of the lightest state with which the operator has a nonzero overlap. If the effective mass is nonmonotonously decreasing, the spectral function has necessarily negative contributions. Therefore it then does not describe a physical particle.

Because of the larger systematic uncertainties, especially with respect to discretization, the interpretation of these quantities is more involved than in the fundamental case. In the latter case [23], the effective masses approached at long times a, more or less, physical behavior, indicating a would-be pole mass of about 200–250 MeV, with indications of positivity violations remaining at short times. The only necessity was to be sufficiently close to the thermodynamic limit to observe a universal behavior.

Due to the same effects which already plagued the extraction of the screening mass in Sec. IV A, this is no longer the case. To actually observe a unique behavior requires to work at fixed lattice spacing. Even then, a substantial finite-volume effect remains. As an illustration, in Figs. 22–24 the effective mass (8) is shown at fixed $a^{-1} \approx 1.5$ GeV in two, three, and four dimensions, respectively. As in the fundamental case [23], the effective mass rises at short times, showing again that the particle is unphysical. The finite-volume then eventually makes it fall again. With increasing volume, the effective mass becomes flatter and flatter over a longer period of time, again similar to the fundamental case.

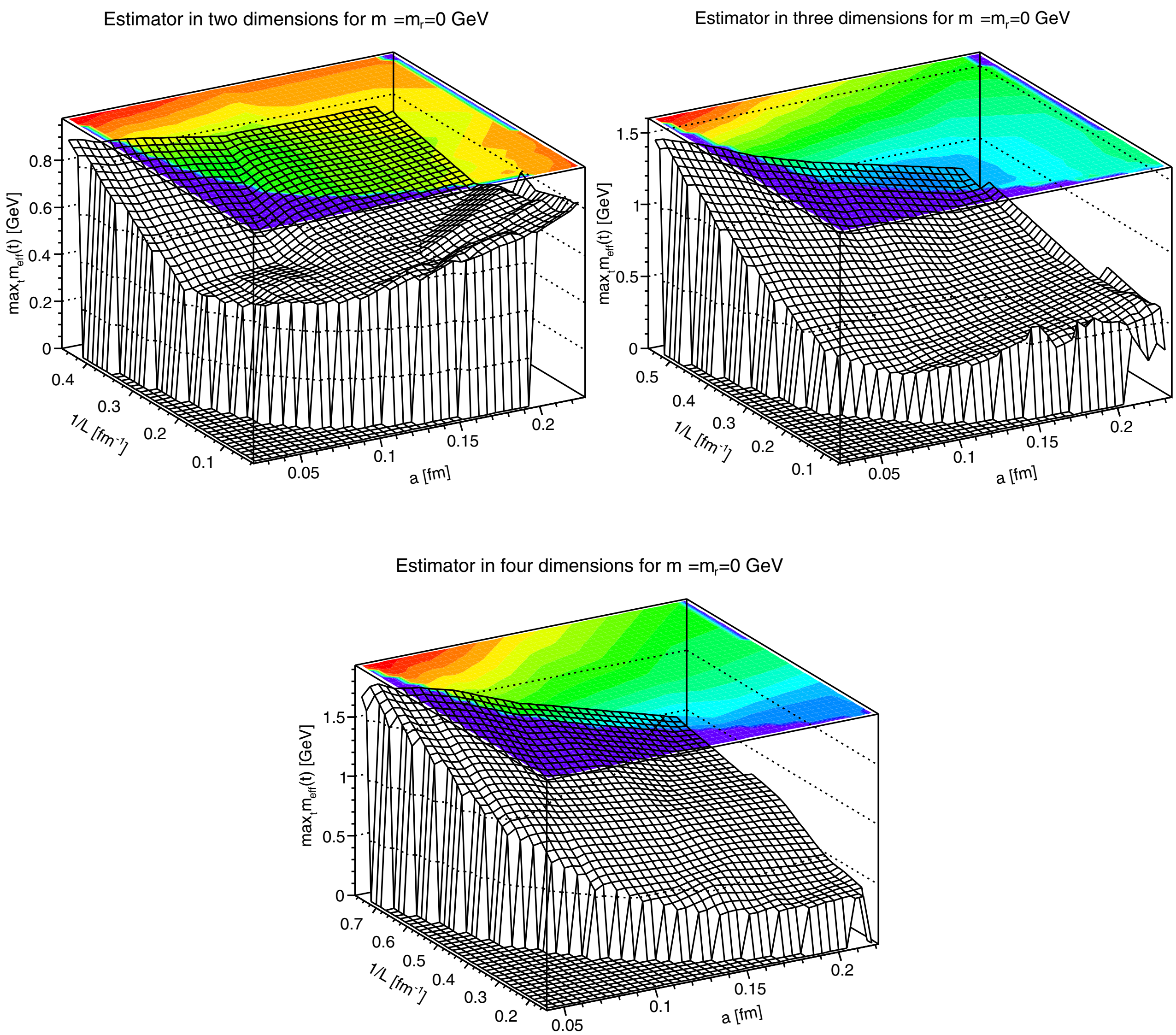

FIG. 25. The maximum of the effective mass (8) in two dimensions (top-left panel), three dimensions (top-right panel), and four dimensions (bottom panel) as a function of lattice size and lattice spacing.

Thus, the maximum effective mass can be used as an estimator for an upper limit of such a would-be long-time pole mass. The result at $m = m_r = 0$ GeV for this quantity is shown in Fig. 25. In all cases, the estimator is strongly affected by the lattice parameters. In two dimensions, the estimator flattens out at about 500 MeV at sufficiently small lattice spacings and large volumes. In higher dimensions, it shows a complex combination of trends, dropping at least below 400 MeV closest to the thermodynamic limit. The results in three dimensions suggest that this process may come to a finite value in the thermodynamic limit. In four dimensions, this is harder to judge. It is hence far less obvious if the adjoint scalar resembles at least for some distance regime a physical, massive particle as it was in the fundamental case [23].

The situation is quite similar for $m = m_r = 0.1$ GeV, and indeed leading to similar quantitative effects. Especially, the values for the estimator are essentially identical, and no trace of the differing renormalized masses remain. Quite contrary at $m = m_r = 1$ GeV the same estimator is within some 10% independent of the lattice parameters, and quickly converges to 1 GeV. Thus, no additional contribution to this mass estimator is observed. This is as in the fundamental case [23]. Hence, a large explicit mass completely overpowers any other contribution. For the largest mass, a rise towards its value is also seen, but as the values of a^{-1} are still below its value, this does not flatten out.

From this, it can be concluded that there appears to be in the adjoint case an additional mass generated. But because of much stronger lattice artifacts, this needs to be handled with much more care than in the fundamental case. Also, its value of about 400 MeV is not so much larger than the 250 MeV observed in the fundamental case as the

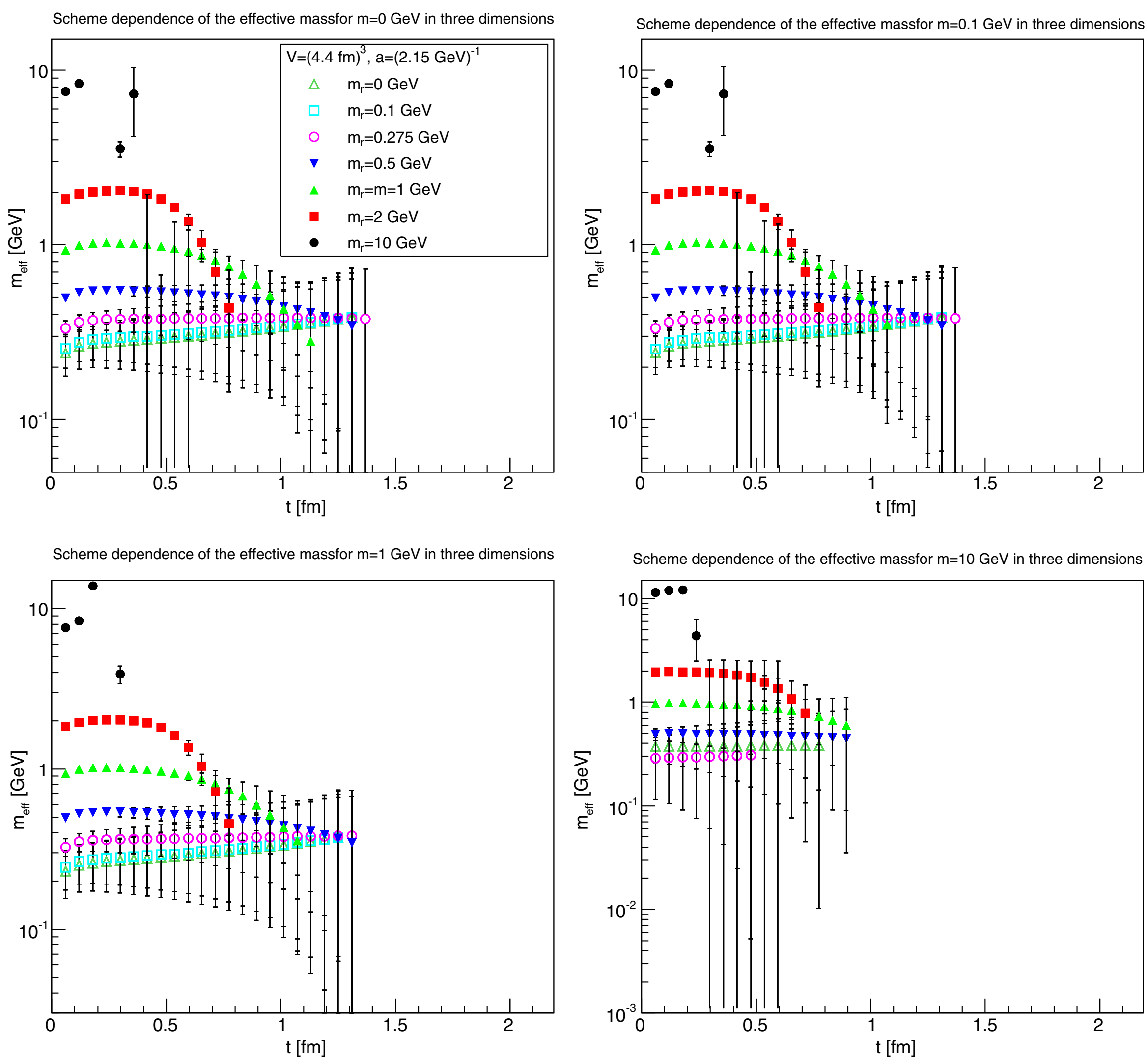

FIG. 26. The effective mass (8) in three dimensions for different renormalization schemes. The top-left panel shows the case of $m = m_r = 0$ GeV, the top-right panel of $m = m_r = 0.1$ GeV, the bottom-left panel of $m = m_r = 1$ GeV, and the bottom-right panel of $m = m_r = 10$ GeV. Points with more than 100% relative error are suppressed.

difference between fundamental fermions and adjoint fermions suggest.

Finally, an investigation of the scheme dependence along the lines of [23] reveals the same pattern: It is possible to shift the effective mass around, but it is not possible to push it below a certain limit, no matter the tree-level mass. This lower limit is similar for all tree-level masses and of the same size as those shown in Fig. 25; i.e., just as in perturbation theory, this effective mass remains not a physical quantity but scheme dependent. Interestingly, as is shown in Fig. 26, the flatness, of the effective mass curve is affected by the choice of renormalization scheme. There exists a "sweet spot" in the example at about 275 MeV, where the effective mass becomes almost flat, except at very short times. Thus, there exists a scheme, which makes the adjoint scalar most "particlelike." Note that this value is actually independent from the tree-level mass. This mass value is also a value consistent with where the estimator in Fig. 25 are moving to in the thermodynamic limit.

As a flat curve would correspond to a physical particle of this mass, the best interpretation of this observation is that at this value of m_r the renormalization scheme becomes the closest approximation to a pole scheme.

V. CONCLUSION

Summarizing, the propagator of an adjoint scalar in the quenched approximation has been studied in detail in two, three, and four dimensions. It shows both stronger modifications compared to its tree-level form as well as much stronger influences of lattice artifacts in comparison to a fundamental scalar [23]. Still, despite all quantitative differences, there appears to be little qualitative difference between both cases. Especially, in both cases a dynamical scale generation of about a few hundred MeV has been observed, independent of the tree-level mass. Moreover, neither particle exhibits a behavior which looks like a physical particle, though both approximate such a behavior at long distances. In the present adjoint case, this is much more sensitive to renormalization effects and lattice artifacts.

What is not seen is any indication, as was originally hoped for, which hint to an obvious connection to (Wilson) confinement. While the fundamental and adjoint Wilson string show, at the distance scales achieved here, qualitative different behavior in sufficiently high dimensions, this is not the case for the propagators. Especially the string breaking in the adjoint case seems to have no direct impact.

Also, there is no difference seen for the different dimensionality. Even though the physical picture, due to geometric Wilson confinement or the possibility of triviality in the dynamical case as allured to in the introduction, differs substantially between different dimensions, this seems to have next to no qualitative impact on the propagator. In fact, even quantitatively, there is very little difference in the different dimensions.

While the present study cannot exclude some more subtle hint in the propagators, the lack of any obvious effect is unfortunate, especially when searching for a possibility to obtain such information from low-order correlation functions. It may still be that such information is hidden in the vertices, as has been variously suggested [15,49–51]. Thus, a study of the corresponding vertices is a logical next step [20,52].

ACKNOWLEDGMENTS

This work was supported by the DFG under Grants No. MA 3935/5-1 and No. MA-3935/8-1 (Heisenberg program) and the FWF under Grant No. M1099-N16. Simulations were performed on the HPC clusters at the Universities of Jena and Graz. The author is grateful to the HPC teams for the very good performance of the clusters. The ROOT framework [53] has been used in this project.

APPENDIX: LATTICE SETUPS

The various lattice setups are listed in Table III. The determination of the lattice spacings has been performed as in [32].

TABLE III. Number and parameters of the configurations used, ordered by dimension, lattice spacing, and physical volume. In all cases, $2(10N + 100(d-1))$ thermalization sweeps and $2(N + 10(d-1))$ decorrelation sweeps of mixed updates [38] have been performed, and auto-correlation times of local observables have been monitored to be at or below one sweep. The number of configurations were selected such as to have a reasonable small statistical error for the renormalization constants determined in Sec. III. The value m_0 denotes the value of the mass parameter in (1) to yield a tree-level mass of 1 GeV. The other tree-level masses are obtained by multiplying or dividing this number by 10, or setting it to zero for tree-level mass zero.

d	N	β	a [fm]	a^{-1} [GeV]	L [fm]	m_0	Config.
2	92	6.23	0.228	0.863	21	1.159	4994
2	106	6.33	0.226	0.870	24	1.149	5440
2	80	6.40	0.225	0.875	18	1.143	3957
2	58	6.45	0.224	0.879	13	1.138	3386
2	18	6.55	0.222	0.886	4.0	1.129	3661
2	122	6.60	0.221	0.890	27	1.124	4750
2	34	6.64	0.221	0.893	7.5	1.120	2970
2	68	6.64	0.221	0.893	15	1.120	3456
2	10	6.68	0.220	0.895	2.2	1.117	2192
2	50	6.68	0.220	0.895	11	1.117	3299
2	26	6.72	0.219	0.898	5.7	1.113	3410
2	42	6.73	0.219	0.900	9.2	1.112	3370
2	106	8.13	0.198	0.994	21	1.006	5440
2	122	8.24	0.197	1.00	24	0.9990	5614
2	92	8.33	0.196	1.01	18	0.9933	4104
2	68	8.70	0.191	1.03	13	0.9708	3456
2	58	8.83	0.190	1.04	11	0.9632	3386
2	80	9.03	0.188	1.05	15	0.9519	3597

(Table continued)

TABLE III. *(Continued)*

d	N	β	a [fm]	a^{-1} [GeV]	L [fm]	m_0	Config.
2	50	9.36	0.184	1.07	9.2	0.9341	3174
2	42	9.91	0.179	1.10	7.5	0.9066	3433
2	122	10.6	0.172	1.14	21	0.8752	5248
2	106	10.9	0.170	1.16	18	0.8625	4768
2	34	11.1	0.168	1.17	5.7	0.8543	2950
2	92	11.7	0.164	1.20	15	0.8312	4994
2	80	11.8	0.163	1.21	13	0.8275	3498
2	68	11.9	0.162	1.21	11	0.8239	3456
2	58	12.4	0.159	1.24	9.2	0.8065	3304
2	26	13.1	0.154	1.28	4.0	0.7838	3410
2	50	13.8	0.150	1.31	7.5	0.7629	3174
2	122	14.3	0.148	1.34	18	0.7490	5248
2	92	15.5	0.142	1.39	13	0.7185	4930
2	106	15.5	0.142	1.39	15	0.7185	5872
2	80	16.3	0.138	1.43	11	0.7001	2279
2	42	16.8	0.136	1.45	5.7	0.6893	3350
2	68	16.9	0.135	1.46	9.2	0.6872	3420
2	58	18.4	0.130	1.52	7.5	0.6578	3304
2	122	20.3	0.123	1.60	15	0.6254	2106
2	106	20.4	0.123	1.60	13	0.6239	4032
2	18	20.6	0.122	1.61	2.2	0.6208	3660
2	92	21.5	0.120	1.65	11	0.6074	4420
2	34	22.2	0.118	1.67	4.0	0.5974	2970
2	80	23.2	0.115	1.71	9.2	0.5841	3498
2	50	23.6	0.114	1.73	5.7	0.5791	3351
2	68	25.2	0.110	1.79	7.5	0.5600	3420
2	122	26.9	0.107	1.85	13	0.5417	2106
2	106	28.4	0.104	1.90	11	0.5269	5200
2	92	30.5	0.100	1.97	9.2	0.5082	4234
2	58	31.6	0.0983	2.00	5.7	0.4991	3300
2	42	33.6	0.0953	2.07	4.0	0.4838	3680
2	80	34.7	0.0938	2.10	7.5	0.4759	3498
2	122	37.4	0.0903	2.18	11	0.4582	4372
2	106	40.4	0.0868	2.27	9.2	0.4406	4592
2	26	42.4	0.0847	2.33	2.2	0.4300	2720
2	68	43.2	0.0839	2.35	5.7	0.4260	3505
2	92	45.7	0.0816	2.42	7.5	0.4140	3848
2	50	47.4	0.0801	2.46	4.0	0.4064	3215
2	122	53.3	0.0755	2.61	9.2	0.3831	4698
2	80	59.7	0.0713	2.76	5.7	0.3618	3505
2	106	60.5	0.0708	2.78	7.5	0.3593	4240
2	58	63.7	0.0690	2.86	4.0	0.3501	3276
2	34	72.3	0.0647	3.04	2.2	0.3285	3549
2	92	78.8	0.0620	3.18	5.7	0.3146	4848
2	122	80	0.03122	3.20	7.5	0.3122	4896
2	68	87.3	0.0589	3.35	4.0	0.2988	3472
2	106	104	0.0539	3.65	5.7	0.2736	4474
2	42	110	0.0524	3.76	2.2	0.2660	3122
2	80	120	0.0502	3.93	4.0	0.02546	3631
2	50	155	0.0441	4.47	2.2	0.2239	3105
2	92	159	0.0436	4.52	4.0	0.2211	4110
2	58	209	0.0380	5.19	2.2	0.1928	3304
2	106	211	0.0378	5.21	4.0	0.1919	5184
2	68	287	0.0324	6.08	2.2	0.1644	3716
2	80	398	0.0275	7.16	2.2	0.1396	3509
2	92	526	0.0239	8.24	2.2	0.1214	5664

(Table continued)

TABLE III. *(Continued)*

d	N	β	a [fm]	a^{-1} [GeV]	L [fm]	m_0	Config.
2	106	698	0.0208	9.49	2.2	0.1054	2784
3	60	3.30	0.234	0.841	14	1.189	2752
3	74	3.34	0.231	0.854	17	1.170	2225
3	48	3.35	0.230	0.858	11	1.166	3654
3	66	3.37	0.228	0.864	15	1.157	2816
3	8	3.40	0.225	0.874	1.8	1.144	3000
3	54	3.43	0.223	0.884	12	1.131	5623
3	14	3.44	0.222	0.887	3.1	1.127	3600
3	20	3.46	0.220	0.894	4.4	1.119	3160
3	26	3.47	0.220	0.897	5.7	1.115	2840
3	36	3.47	0.220	0.897	7.9	1.115	3300
3	42	3.47	0.220	0.897	9.2	1.115	5021
3	32	3.48	0.219	0.900	7.0	1.111	2996
3	66	3.56	0.213	0.927	14	1.079	2200
3	54	3.68	0.204	0.966	11	1.035	5538
3	74	3.69	0.203	0.969	15	1.032	2225
3	60	3.73	0.201	0.982	12	1.018	2752
3	36	3.82	0.195	1.01	7.0	0.9883	3462
3	48	3.86	0.192	1.03	9.2	0.9756	3654
3	74	3.90	0.190	1.04	14	0.9632	2225
3	42	3.92	0.189	1.04	7.9	0.9572	3450
3	60	4.01	0.183	1.07	11	0.9308	2752
3	66	4.03	0.182	1.08	12	0.9251	2816
3	32	4.10	0.178	1.10	5.7	0.9058	3006
3	54	4.25	0.171	1.15	9.2	0.8671	5304
3	26	4.28	0.169	1.16	4.4	0.8597	2840
3	42	4.33	0.167	1.18	7.0	0.8477	3277
3	66	4.33	0.167	1.18	11	0.8477	2200
3	48	4.38	0.165	1.20	7.9	0.8360	4776
3	74	4.43	0.162	1.21	12	0.8247	2225
3	54	4.83	0.147	1.34	7.9	0.7439	3744
3	48	4.84	0.146	1.35	7.0	0.7420	3600
3	36	4.52	0.159	1.24	5.7	0.8050	3300
3	20	4.60	0.155	1.27	3.1	0.7883	3160
3	60	4.64	0.154	1.28	9.2	0.7802	2496
3	74	4.77	0.149	1.32	11	0.7550	2848
3	66	5.03	0.140	1.41	9.2	0.7091	2160
3	32	5.09	0.138	1.43	4.4	0.6993	3070
3	42	5.15	0.136	1.45	5.7	0.6897	3400
3	60	5.29	0.132	1.50	7.9	0.6685	4602
3	54	5.36	0.130	1.52	7.0	0.6583	8312
3	14	5.39	0.129	1.53	1.8	0.6540	3600
3	74	5.55	0.125	1.58	9.2	0.6322	2560
3	36	5.64	0.122	1.61	4.4	0.6206	3300
3	66	5.74	0.120	1.64	7.9	0.6081	4338
3	26	5.76	0.119	1.65	3.1	0.6057	2768
3	48	5.78	0.119	1.66	5.7	0.6033	2485
3	60	5.87	0.117	1.69	7.0	0.5927	2015
3	74	6.34	0.107	1.84	7.9	0.5428	2560
3	66	6.38	0.106	1.86	7.0	0.5389	2112
3	54	6.41	0.106	1.87	5.7	0.5361	3893
3	42	6.45	0.105	1.88	4.4	0.5323	3450
3	32	6.91	0.0970	2.03	3.1	0.4925	3070
3	60	7.04	0.0950	2.07	5.7	0.4824	4050
3	74	7.06	0.0947	2.08	7.0	0.4808	2560
3	48	7.27	0.0917	2.15	4.4	0.4653	5166

(Table continued)

TABLE III. *(Continued)*

d	N	β	a [fm]	a^{-1} [GeV]	L [fm]	m_0	Config.
3	20	7.39	0.0900	2.19	1.8	0.4569	3160
3	66	7.67	0.0864	2.28	5.7	0.4384	4400
3	36	7.69	0.0861	2.29	3.1	0.4371	3387
3	54	8.08	0.0815	2.42	4.4	0.4139	3931
3	42	8.84	0.0739	2.67	3.1	0.3750	5359
3	60	8.89	0.0734	2.68	4.4	0.3727	2496
3	26	9.38	0.0692	2.84	1.8	0.3515	2840
3	66	9.71	0.0667	2.95	4.4	0.3386	2560
3	48	10.0	0.0646	3.05	3.1	0.3280	3894
3	74	10.8	0.0595	3.31	4.4	0.3019	2560
3	54	11.1	0.0577	3.41	3.1	0.2931	4973
3	32	11.3	0.0566	3.48	1.8	0.2875	3208
3	60	12.3	0.0517	3.81	3.1	0.2627	1892
3	36	12.7	0.0500	3.94	1.8	0.2539	3410
3	66	13.4	0.0472	4.17	3.1	0.2398	2450
3	42	14.6	0.0432	4.57	1.8	0.2191	3357
3	48	16.6	0.0377	5.22	1.8	0.1914	3769
3	54	18.6	0.0335	5.88	1.8	0.1700	4548
3	60	20.6	0.0301	6.54	1.8	0.01529	4381
3	66	22.6	0.0274	7.20	1.8	0.01389	2464
3	74	25.3	0.0244	8.09	1.8	0.01236	2464
4	14	2.179	0.221	0.889	3.1	1.124	2930
4	10	2.181	0.220	0.894	2.2	1.119	3000
4	26	2.183	0.219	0.898	5.7	1.114	3152
4	22	2.185	0.218	0.902	4.8	1.109	3186
4	6	2.188	0.217	0.908	1.3	1.101	2220
4	18	2.188	0.217	0.908	3.9	1.101	3284
4	30	2.188	0.217	0.908	6.5	1.101	3000

(Table continued)

TABLE III. *(Continued)*

d	N	β	a [fm]	a^{-1} [GeV]	L [fm]	m_0	Config.
4	32	2.190	0.216	0.912	6.9	1.096	1646
4	30	2.241	0.190	1.03	5.7	0.9667	3639
4	26	2.252	0.185	1.06	4.8	0.9396	3406
4	32	2.266	0.178	1.10	5.7	0.9055	3495
4	22	2.268	0.177	1.11	3.9	0.9007	3096
4	18	2.279	0.172	1.14	3.1	0.8743	3277
4	30	2.305	0.160	1.23	4.8	0.8136	4152
4	14	2.311	0.158	1.25	2.2	0.7999	2910
4	26	2.328	0.150	1.31	3.9	0.7618	3256
4	32	2.328	0.150	1.31	4.8	0.7618	2128
4	22	2.349	0.141	1.40	3.1	0.7162	2996
4	10	2.376	0.130	1.52	1.3	0.6600	3000
4	30	2.376	0.130	1.52	3.9	0.6600	3412
4	18	2.395	0.123	1.61	2.2	0.6222	3105
4	32	2.396	0.122	1.61	3.9	0.6203	2430
4	26	2.403	0.120	1.65	3.1	0.6067	3253
4	30	2.448	0.103	1.91	3.1	0.5246	3380
4	22	2.457	0.100	1.96	2.2	0.5092	3052
4	32	2.467	0.0970	2.03	3.1	0.4925	1797
4	14	2.480	0.0929	2.12	1.3	0.4714	2930
4	26	2.507	0.0847	2.33	2.2	0.4299	3239
4	30	2.548	0.0734	2.68	2.2	0.3726	3434
4	18	2.552	0.0724	2.72	1.3	0.3674	3280
4	32	2.566	0.0689	2.86	2.2	0.03496	4235
4	22	2.609	0.0591	3.33	1.3	0.3001	3252
4	26	2.656	0.0501	3.93	1.3	0.2543	3706
4	30	2.698	0.0434	4.54	1.3	0.2204	3593
4	32	2.718	0.0407	4.84	1.3	0.2065	2020

[1] R. Alkofer and J. Greensite, J. Phys. G **34**, S3 (2007).
[2] R. Alkofer and L. von Smekal, Phys. Rep. **353**, 281 (2001).
[3] A. Maas, Phys. Rep. **524**, 203 (2013).
[4] C. S. Fischer, J. Phys. G **32**, R253 (2006).
[5] D. Binosi and J. Papavassiliou, Phys. Rep. **479**, 1 (2009).
[6] P. Boucaud, J. P. Leroy, A. Le Yaouanc, J. Micheli, O. Pène, and J. Rodríguez-Quintero, Few-Body Syst. **53**, 387 (2012).
[7] N. Vandersickel and D. Zwanziger, Phys. Rep. **520**, 175 (2012).
[8] C. D. Roberts, J. Phys. Conf. Ser. **706**, 022003 (2016).
[9] S. Strauss, C. S. Fischer, and C. Kellermann, Phys. Rev. Lett. **109**, 252001 (2012).
[10] A. Cucchieri, D. Dudal, T. Mendes, and N. Vandersickel, Phys. Rev. D **93**, 094513 (2016).
[11] C. D. Roberts and A. G. Williams, Prog. Part. Nucl. Phys. **33**, 477 (1994).
[12] R. Alkofer, W. Detmold, C. S. Fischer, and P. Maris, Phys. Rev. D **70**, 014014 (2004).
[13] D. August and A. Maas, J. High Energy Phys. 07 (2013) 001.
[14] A. Maas, arXiv:1712.04721.
[15] L. Fister, R. Alkofer, and K. Schwenzer, Phys. Lett. B **688**, 237 (2010).
[16] V. Macher, A. Maas, and R. Alkofer, Int. J. Mod. Phys. A **27**, 1250098 (2012).
[17] M. A. L. Capri, D. Dudal, A. J. Gómez, M. S. Guimaraes, I. F. Justo, S. P. Sorella, and D. Vercauteren, Phys. Rev. D **88**, 085022 (2013).
[18] M. A. L. Capri, D. Dudal, M. S. Guimaraes, I. F. Justo, S. P. Sorella, and D. Vercauteren, Ann. Phys. (Amsterdam) **343**, 72 (2014).
[19] M. Hopfer and R. Alkofer, Acta Phys. Pol. B Proc. Suppl. **6**, 929 (2013).
[20] A. Maas, Proc. Sci., FacesQCD2011 (**2011**) 033.
[21] A. Maas and T. Mufti, J. High Energy Phys. 04 (2014) 006.
[22] M. A. L. Capri, D. Fiorentini, A. D. Pereira, and S. P. Sorella, Eur. Phys. J. C **77**, 546 (2017).
[23] A. Maas, Eur. Phys. J. C **76**, 366 (2016).
[24] A. C. Aguilar and J. Papavassiliou, Phys. Rev. D **83**, 014013 (2011).

[25] T. Maskawa and H. Nakajima, Prog. Theor. Phys. **52**, 1326 (1974).
[26] R. Fukuda and T. Kugo, Nucl. Phys. **B117**, 250 (1976).
[27] F. Karsch and M. Lutgemeier, Nucl. Phys. **B550**, 449 (1999).
[28] J. Engels, S. Holtmann, and T. Schulze, Nucl. Phys. **B724**, 357 (2005).
[29] E. Bilgici, C. Gattringer, E.-M. Ilgenfritz, and A. Maas, J. High Energy Phys. 11 (2009) 035.
[30] A. Maas, Phys. Rev. D **75**, 116004 (2007).
[31] A. Cucchieri and T. Mendes, Phys. Rev. Lett. **100**, 241601 (2008).
[32] A. Maas, Phys. Rev. D **91**, 034502 (2015).
[33] H. G. Dosch and V. F. Muller, Fortschr. Phys. **27**, 547 (1979).
[34] D. J. E. Callaway, Phys. Rep. **167**, 241 (1988).
[35] A. Maas, R. Sondenheimer, and P. Törek, Ann. Phys. (Amsterdam) **402**, 18 (2019).
[36] K. Olynyk and J. Shigemitsu, Phys. Rev. Lett. **54**, 2403 (1985).
[37] I.-H. Lee and J. Shigemitsu, Nucl. Phys. **B263**, 280 (1986).
[38] A. Cucchieri, A. Maas, and T. Mendes, Phys. Rev. D **74**, 014503 (2006).
[39] A. Maas, Eur. Phys. J. C **71**, 1548 (2011).
[40] A. Maas, Eur. Phys. J. C **75**, 122 (2015).
[41] J. Greensite, A. V. Kovalenko, Š. Olejník, M. I. Polikarpov, S. N. Syritsyn, and V. I. Zakharov, Phys. Rev. D **74**, 094507 (2006).
[42] A. Sternbeck, K. Maltman, M. Müller-Preussker, and L. von Smekal, Proc. Sci., LATTICE2012 (**2012**) 243.
[43] P. Boucaud, F. De Soto, J. P. Leroy, A. Le Yaouanc, J. Micheli, O. Pène, and J. Rodríguez-Quintero, Phys. Rev. D **79**, 014508 (2009).
[44] M. Böhm, A. Denner, and H. Joos, *Gauge Theories of the Strong and Electroweak Interaction* (Teubner, Stuttgart, 2001).
[45] R. Oehme and W. Zimmermann, Phys. Rev. D **21**, 471 (1980).
[46] V. Mathieu, N. Kochelev, and V. Vento, Int. J. Mod. Phys. E **18**, 1 (2009).
[47] R. Jackiw and S. Templeton, Phys. Rev. D **23**, 2291 (1981).
[48] E. Seiler, *Gauge Theories as a Problem of Constructive Quantum Field Theory and Statistical Mechanics*, Lecture Notes in Physics (Springer-Verlag, Berlin Heidelberg, 1982).
[49] R. Alkofer, C. S. Fischer, and F. J. Llanes-Estrada, Phys. Lett. B **611**, 279 (2005).
[50] R. Alkofer, C. S. Fischer, F. J. Llanes-Estrada, and K. Schwenzer, Ann. Phys. (Amsterdam) **324**, 106 (2009).
[51] D. Zwanziger, Phys. Rev. D **81**, 125027 (2010).
[52] A. Maas (to be published).
[53] R. Brun and F. Rademakers, Nucl. Instrum. Methods Phys. Res., Sect. A **389**, 81 (1997).